Chapter 20
Solid-State Thin-Film Lithium Batteries for Integration in Microsystems

J.F. Ribeiro, M.F. Silva, J.P. Carmo, L.M. Gonçalves, M.M. Silva, and J.H. Correia

Abstract The increasing miniaturization of electronic devices requires the miniaturization of devices that provide energy to them. Autonomous devices of reduced energy consumption are increasingly common and they have benefited from energy harvesting techniques. However, these devices often have peak power consumption, requiring storage of energy.

This chapter presents the fabrication and characterization of thin-films for solid-state lithium battery. The solid-state batteries stand out for the possibility of all materials being solid and therefore ideal for microelectronics fabrication techniques. Lithium batteries are composed primarily of three materials, the cathode, the electrolyte and the anode. The positive electrode (cathode) and negative (anode) have high electrical conductivity and capacity for extraction and insertion of lithium ions. The electrolyte's main features are the high ionic conductivity and high electrical resistivity. The materials chosen for the battery are lithium cobalt oxide (cathode), lithium phosphorus oxynitride (electrolyte), and metallic lithium (anode).

The lithium cobalt oxide cathode ($LiCoO_2$) was deposited by RF sputtering and characterized using the XRD, EDX, SEM techniques, and electrical resistivity. Fully crystalline $LiCoO_2$ was achieved with an annealing of 650°C in vacuum for 2 h. Electrical resistivity of 3.7 Ω·mm was achieved.

The lithium phosphorus oxynitride electrolyte (LIPON) was deposited by RF sputtering and characterized using the techniques EDX, SEM, ionic conductivity, DSC, and TGA. Ionic conductivity of 6.3×10^{-7} S · cm^{-1} for a temperature of 26°C was measured. The thermal stability of LIPON up to 400°C was also proved.

The metallic lithium anode (Li) was deposited by thermal evaporation and its electrical resistance measured at four points during the deposition. Resistance of about 3.5 Ω was measured for a thickness of 3 μm. The oxidation rate of the lithium in contact with the ambient atmosphere was evaluated. The patterning process of the battery was developed by means of shadow masks.

B. Bhushan (ed.), *Scanning Probe Microscopy in Nanoscience and Nanotechnology 3*, NanoScience and Technology, DOI 10.1007/978-3-642-25414-7_20,

20.1 Introduction

20.1.1 Thin-Film Batteries

A battery is an energy source that converts chemical energy into electrical energy [1]. Each battery consists of an electrolyte and two electrodes. The electrolyte is essentially an excellent ionic conductor and an excellent electrical insulator. The electrodes are designated as cathode (positive electrode) and anode (negative electrode) and are essentially good electrical conductors, capable of insertion and extraction of ions. The battery produces electric current when an atom or molecule becomes an ion by electron transfer [2]. The electron is released into an external circuit via an oxidation reaction. The ion resulting from the oxidation reaction will flow through the electrolyte and a counter reaction, the reduction will occur at the cathode. The electron transfer reactions, known as redox reactions, occur among a set of chemical species. In the case of the battery, the anode is the reducer and the cathode is the oxidant, in other words, the anode gives electrons and the cathode has the capacity to receive them. The change between the types of charge carriers, i.e., the electrolyte and the electrode, forces the reaction between the electrode/electrolyte connection [3]. Figure 20.1 shows a simplified schematic of a battery.

The power provided to an external circuit through redox reactions is called battery discharge. The redox reaction is possible only when a battery cathode and anode have different chemical potentials [2]. The chemical potential is equivalent to the electric potential in an electronic circuit by analogy. The chemical potential of a material is the partial molar free energy of Gibbs of this element in a solution [4]. Thus we can consider it to be the driving force for the diffusion of atoms in a broad sense of the word. The battery is rechargeable when the cathode and anode also have the capacity to release and receive electrons respectively. Recharging the battery takes place by applying a reverse voltage higher than the operating voltage of the battery, thereby forcing the electrons and ions to flow back to the battery anode. This process is called charging the battery.

20.1.2 Battery Evolution

The electric battery was invented by Alessandro Volta (Fig. 20.2) in late 1799 [5], who announced his invention to the Royal Society of London in 1800. The investigation that led to the development of this device began in 1792, after Volta read the work of Luigi Galvani [6]. The work of Galvani reported the existence of intrinsic electricity in living organisms [7].

In 1802, Dr. William Cruickshank designed the first electric battery capable of being mass-produced. Cruickshank had managed to obtain copper sheets in the shape of squares, which were welded to the edge of zinc sheets of the same size. These sheets were placed inside a rectangular wooden box, which was then

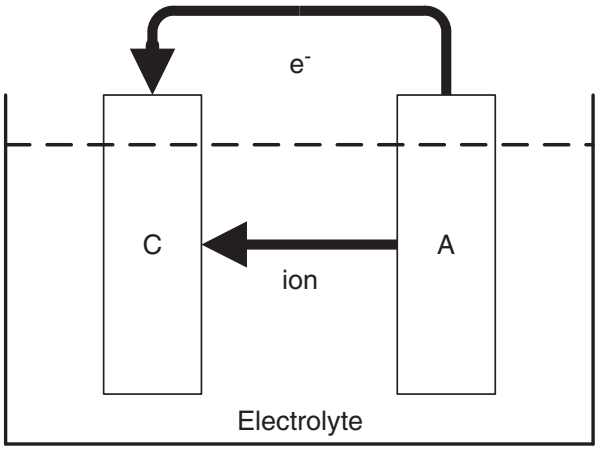

Fig. 20.1 Simplified schematic of battery discharge, where C is the cathode and A is the anode

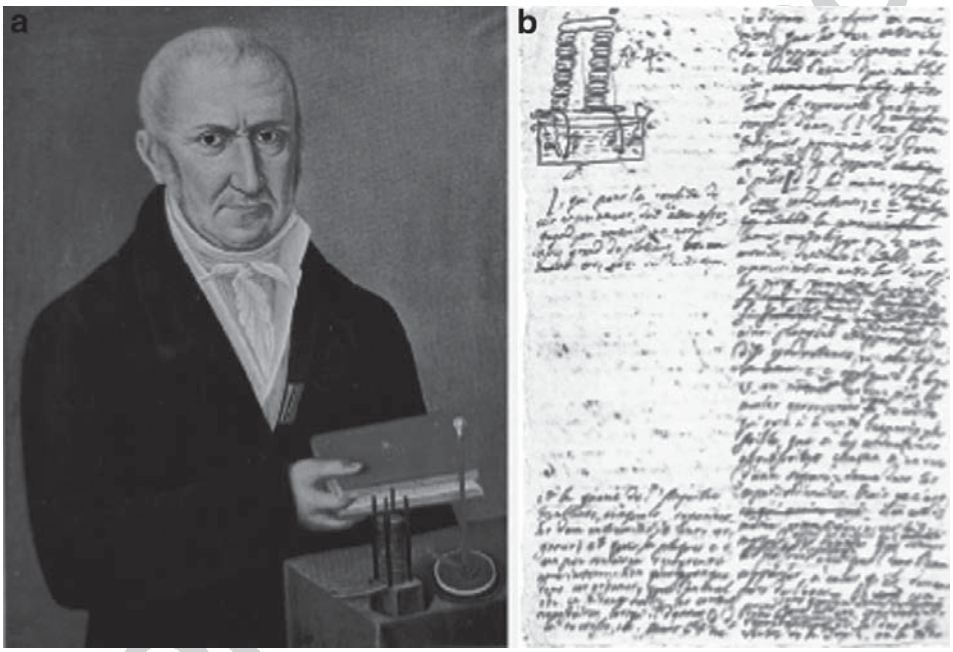

Fig. 20.2 Alessandro Volta: (**a**) contemporary picture, (**b**) letter of page that announced the electric battery [8]

sealed with cement. After putting the plates in position, the box was filled with an electrolyte of brine solution (water saturated with salt). John F. Daniell, an English chemist, developed in 1836, a battery with a better and more stable current than the device of Volta. He tried to find a solution to the problem of hydrogen bubbles found in the Volta battery, adding a second electrolyte to consume hydrogen [6]. In 1844, William Robert Grove developed a battery with a higher current than that of Daniell and nearly twice the voltage. This consisted of a platinum cathode immersed in nitric acid and a zinc anode immersed in sulfuric acid, separated by porous clay.

Gaston Planté, a French physicist, invented the first rechargeable battery in 1859. This battery was based on lead-acid chemistry that is still used [9]. During the 1860s came a variant of the Daniell battery, invented by Callaud, which dispensed with the porous barrier that allowed the increase of current. In 1866, Georges

Leclanché invented a battery with a manganese dioxide cathode, a zinc anode, and an electrolyte of ammonium chloride, known as the Leclanché battery. Several scientists have tried to find a battery consisting of only solid materials for ease of use. Carl Gassner in 1886 obtained a German patent of a variant of the Leclanché battery, which came to be known as the dry battery, because the electrolyte was not a free liquid [6].

In 1899, Waldmar Jungner from Sweden invented the nickel-cadmium battery, with nickel as the positive electrode, cadmium the negative electrode, and an electrolyte solution of potassium hydroxide [9]. Two years later, Edison replaced cadmium by iron forming the nickel-iron battery. At this point, the nickel-cadmium and nickel-iron was expensive due to the cost of their materials and therefore had limited applications. The nickel cadmium batteries became available only after Shlecht and Ackermann improved the load current and longevity of batteries in 1932, and after Neumann completely sealed the batteries in 1947 [6].

Lewis Urry, an engineer who worked for Energizer, was given the task of improving the longevity of the zinc-carbon battery. Urry decided that this was not the best solution and dedicated his time to the development of alkaline batteries with a manganese dioxide cathode, an anode of zinc powder, and an alkaline electrolyte [10]. This battery became commercially available in 1959. The batteries of nickel metal hydride appeared in the market in 1989 as a variation of the nickel-hydrogen batteries, which had appeared in 1970.

The early research on lithium secondary batteries dates back to the years of 1960–1970 due to the energy crisis and the growing interest in energy sources for mobile applications [6]. However, no breakthrough was achieved until 1991 and there is still a major deficiency in the power and energy density of secondary batteries. John B. Goodenough, in 1980, led a team in Sony in the investigation of Li-ion batteries. These batteries came into the market in 1991 [11, 12]. The lithium polymer batteries that were launched in 1996 introduced greater flexibility and energy density [13]. Lithium solid state batteries emerged only in 2009, released by the company Cymbet [14]. Table 20.1 summarizes the history of batteries.

Currently most attempts to improve the batteries face the macro scale problem, but work is now being directed to the nano scale [15]. The nano materials were slow to enter into the energy storage market because the effective increase in surface area of the electrodes increases the risk of adverse reactions involving the decomposition of the electrolyte. Only in 2000 was it perceived that such reactions can be controlled by coating the electrodes to protect them from unwanted oxidation and reduction reactions. The work on nano materials gave new life to lithium-ion batteries [16]. Nano materials allow benefits in terms of capacity, power, energy density, and cost of lithium ion batteries and are still far from being fully exploited [15], making it increasingly important for energy storage [17–19]. In the coming decades the batteries may also evolve into using organic materials. Today the feasibility of using $Li_X C_6O_6$ active molecules, which can be prepared from natural sugars, is already under investigation [20].

Table 20.2 presents a comparison between lithium and other battery types. The first column indicates the type of battery; the second indicates the voltage

Table 20.1 Battery history [6]

1600	Gilbert (English)	Established the electrochemical study	t24.1
1791	Galvani (Italian)	Discovered "animal electricity"	t24.2
1800	Volta (Italian)	Electrical battery inventor	t24.3
1802	Cruickshank (English)	First electrical battery capable of mass production	t24.4
1820	Ampère (France)	Electricity through magnetism	t24.5
1833	Faraday (English)	Faraday's law announcement	t24.6
1836	Daniell (English)	Daniell's battery invention	t24.7
1844	Grove (Wales)	Grove's battery invention	t24.8
1859	Planté (France)	Lead-acid battery invention	t24.9
1868	Leclanché (France)	Leclanché's battery invention	t24.10
1888	Gassner (USA)	Dry battery completion	t24.11
1899	Jungner (Sweden)	Nickel-cadmium battery invention	t24.12
1901	Edison (USA)	Nickel-iron battery invention	t24.13
1932	Shlecht and Ackermann (Germany)	Cluster plate invention	t24.14
1947	Neumann (France)	Nickel-cadmium battery successfully sealed	t24.15
1960	Union Carbide (USA)	First alkaline battery development	t24.16
1970		Development of valve regulated for lead-acid batteries	t24.17
1990		Sales of hydride nickel-metal batteries	t24.18
1992	Kordesch (Canada)	Marketing of rechargeable alkaline batteries	t24.19
1999		Marketing of polymer lithium ion batteries	t24.20
2009	Cymbet (USA)	Marketing of solid-state lithium ion batteries	t24.21

Table 20.2 Comparison of lithium batteries with other type of batteries [21]

Battery type	Voltage (V)	Energy density (Wh kg^{-1} – Wh L^{-1})	Discharge time for 5 mm thickness (hh:mm:ss)	Discharge time for 1 mm thickness (hh:mm:ss)	
					t25.1 t25.2 t25.3
Ni-Cd	1.2	40–100	11:15:00	00:05:24	t25.4
Ni-MH	1.2	90–245	27:36:00	00:13:12	t25.5
Ag-Zn	1.5	110–220	24:45:00	00:11:54	t25.6
Li-ion	3.6	155–400	45:00:00	00:21:36	t25.7
Li-polymer	3.6	180–380	42:45:00	00:20:24	t25.8
Thin-film Li-ion	3.6	250–1,000	112:30:00	00:54:00	t25.9

produced and the third the gravimetric energy density (Wh/kg) and volumetric energy density (Wh/L) reached with the respective type of battery. The fourth and fifth column show the maximum discharge time at constant current for the battery depending on thickness. 129 130 131 132

20.1.3 Motivation For Thin-Film Batteries 133

One of the great challenges of the twenty-first century is undoubtedly the production and storage of energy. The increased reduction in energy consumption by electronic 134 135

Fig. 20.3 Design of a thin-film battery

devices, either in current or voltage supply, has allowed the creation of autonomous wireless devices without needed external power supply. The wireless autonomous devices have also benefited from the improvement of energy harvesting techniques, which allow the use of various types of energy from the environment (heat, light, vibration, etc.). However these devices require a battery capable of powering the circuit when the power source is not available and permits the leveling of energy consumption, since wireless devices have peak consumption when they are transmitting information and very low power consumption in the remaining period of time.

The need for remote electronic devices is increasing and batteries increasingly play a key role in the viability and minimum size of these same devices. Thus, the integration of the battery in the microchip increases the electronic circuit integration and miniaturization of devices, enabling further cost reduction. Lithium batteries have been highlighted by the possibility of all materials being solid such that they are ideal for fabrication using thin-film techniques, allowing their integration in integrated circuits. The solid-state batteries (all constituent materials are solid) are intrinsically safe, can withstand temperatures of welding and present faster time of charge/discharge than conventional batteries. These batteries can also be manufactured in any shape and size without increasing costs in miniaturization of the same. Figure 20.3 illustrates a possible design for solid-state lithium batteries, using lithium cobalt oxide ($LiCoO_2$) as cathode, the lithium phosphorus oxynitride (LIPON) as electrolyte, and metallic lithium as anode.

20.1.4 Applications

Thin-film batteries have a high range of applications, like energy harvesting modules, wireless sensors, and medical devices. This kind of battery is especially profitable for remote and autonomous devices. Nowadays most remote devices are size- and life-limited by their battery. Conventional batteries are normaly huge in comparison with most electronic remote devices and take a very long time to get charged making it difficult to use the applications of energy harvesting power sources. Thin-film batteries can be charged/discharged in less than a minute.

20.2 Lithium Batteries

20.2.1 Solid-State Batteries

In conventional batteries the electrolyte is usually an acid or an alkaline solution containing dissolved metal ions or an organic solvent consisting of salts with metal ions [2]. Liquid electrolytes have advantages such as high ionic conductivity, high electrical resistivity, and excellent contact with the electrodes. Despite the advantages, liquid electrolytes have serious disadvantages such as corrosion of the electrodes. Batteries with liquid electrolytes also require an airtight package to ensure its security and stability. This type of encapsulation adds weight and reduces the energy density of a battery.

A solid-state electrolyte, in addition to ensuring a high ionic conductivity and high electrical resistance, must ensure good contact and good chemical stability with the electrodes [2]. An excellent energy density can be achieved with solid-state batteries, because of the reduced size and encapsulation of the battery [21].

20.2.2 State of the Art

The thin-film batteries emerged in 1982 [21], when the Japanese company Hitachi announced a thin-film solid-state battery. The advertised battery comprised a cathode of TiS_2 deposited by chemical vapor deposition (CVD), an electrolyte of $Li_{3,6}Si_{0,6}P_{0,4}O_4$ deposited by RF sputtering and an anode of metallic lithium deposited by thermal evaporation. It was also tested $WO_3V_2O_5$ as cathode deposited by sputtering in a H_2-Ar plasma [22].

A second approach was the replacement of the liquid electrolyte by a polymer electrolyte. This technology was restricted to large systems (traction power or backup power) because only they can withstand temperatures up to 80°C [23]. Shortly after, several research groups attempted to develop a hybrid electrolyte, in the hope of combining the advantages of the polymer electrolyte without the risks associated with the use of lithium metal. A hybrid electrolyte comprises a polymer matrix with a liquid solvent and a salt. Companies such as Valence and Danionics were involved in the development of polymer batteries, but they never were commercialized on a large scale because of safety issues [21].

In 1991, Sony sold a lithium-ion battery with a $LiCoO_2$ cathode and a carbon anode [11, 12]. This type of lithium-ion batteries had a potential exceeding 3.6 V (three times longer than alkaline batteries) and gravimetric energy densities of 120–150 $Wh\,kg^{-1}$ (two to three times higher than the nickel-cadmium batteries). These batteries have become ideal for portable electronic devices.

The company NTT Group of Japan has also developed thin-film batteries that use $Li_{3,4}V_{0,6}Si_{0,4}O_4$ as electrolyte and $LiCoO_2$ [24] or $LiMn_2O_4$ [25] as cathode, deposited by RF sputtering. The battery has an area of 1 cm^2 with cathode thickness

of 1–5 μm, electrolyte thickness of 1 μm, and lithium anode thickness of 4–8 μm. Thin-film batteries were also developed by the Bellcore and Battery group of companies in 1980. They used an electrolyte of $Li_4P_2S_7$ or $Li_3PO_4 - P_2S_5$, a cathode of TiS_2 and an anode of lithium or LiI. Bellcore also announced a lithium battery with a $LiMn_2O_4$ cathode, an electrolyte of LiBP or lithium phosphorus oxynitride (LIPON), and a metallic lithium anode. The displayed battery operated between 3.5 and 4.3 V and had a capacity of 70 μ A cm^{-2} to more than 150 cycles [26]. A group at Oak Ridge National Laboratory (ORNL), USA, devoted itself to research of thin-film batteries using an electrolyte of LIPON. The LIPON is deposited by RF sputtering with a target of Li_3PO_4 in a nitrogen atmosphere, and shows high stability compared with lithium oxides or sulfates. Despite LIPON being more stable, it has a moderate ionic conductivity of 2.3×10^{-6} S cm^{-1} at room temperature and activation energy of 0.55 eV [27]. The potential curve indicates a range of stability of LIPON from 0 to 5.5 V against a lithium electrode. The battery anode (lithium metal) was deposited by thermal evaporation and the cathode ($LiCoO_2$ or $LiMn_2O_4$) and electrolyte (LIPON) were deposited by RF sputtering. The ORNL group also investigated some combinations of electrodes with the electrolyte LIPON, and achieved a very good performance for voltages between 2 and 5 V, a current density of 10 mA cm^{-2}, and more than 10,000 cycles of charge/discharge [28]. Neudecker et al., researchers from ORNL, reported a Li-free thin film battery, where the lithium anode and the anode current collector are replaced by a single layer of copper [29]. This battery is quite useful when you want to use a type of welder, since lithium has a melting temperature of 178°C [29], which is below the temperature used for the soldering processes. The LIPON is now recognized as a standard solid electrolyte for thin-film batteries and has been used by many groups, especially in private companies in the USA [1]. The LIPON is also used by Park et al. [30], Korea and Baba et al. [31], Iwate University in Japan. Baba et al. reported thin-film batteries with an electrolyte of LIPON, a cathode of V_2O_5 or $LiMn_2O_4$, and an anode of $Li_XV_2O_5$ deposited by RF sputtering. These thin-film batteries (Li-ion batteries) have the advantage of having less complexity in manufacturing and increased safety than with a lithium anode. The disadvantage with Li-ion batteries is the need to charge them before first use, which does not happen with the batteries with a lithium anode. The Baba et al. battery, displays an increased capability when it exceeds 20 cycles of charge/discharge reaching a maximum capacity of 10 μ Ah cm^{-2} [32]. This behavior is attributed to the gradual decrease of resistance between the materials. Baba et al., also proposed a higher battery voltage and higher current by stacking two batteries on the same substrate, allowing the reduction of the battery contacts. This battery operates at a voltage between 3 and 6.5 V and a current of 2μ A cm^{-2} [33].

The development of thin-film batteries has, after almost 30 years of research, led to the development of rechargeable lithium-ion batteries. Table 20.3 shows some of the developed thin-film batteries.

Thin-film batteries manufactured by companies like Cymbet [14] and Infinite Power Solutions are available in the market [41]. Both use technology from ORNL, above. Four battery models are available from Cymbet:

Table 20.3 Thin-film batteries [21]

Cathode	Electrolyte	Anode	Voltage (V)	Current ($\mu A\,cm^{-2}$)	Capacity	Ref.	t26.1
TiS_2	$Li_{3,6}Si_{0,6}P_{0,4}O_4$	Li	2.5	16	45–150 $\mu Ah\,cm^{-2}$	[22]	t26.2
TiS_XO_Y	Li_2SO_4-Li_2O-B_2O_3	Li	2.6	1–60	40–15 $\mu Ah\,cm^{-2}$	[34]	t26.3
V_2O_5	LIPON	LiV_2O_5	3.5–3.6	10	6 $\mu Ah\,cm^{-2}$	[31]	t26.4
$LiMn_2O_4$	LIPON	V_2O_5	3.5–1	>2	18 $\mu Ah\,cm^{-2}$	[32]	t26.5
$LiMn_2O_4$	LiBP-LIPON	Li	3.5–4.5	70	100 $mAh\,g^{-1}$	[35]	t26.6
$LiMn_2O_4$	$Li_{6,1}V_{0,61}Si_{0,39}O_{5,36}$	Li	3.5–5	10	33.3 $\mu Ah\,cm^{-2}$	[25]	t26.7
$LiMn_2O_4$	LIPON	Li	4.5–2,5	2–40	11–81 $\mu Ah\,cm^{-2}$	[36]	t26.8
$LiCoO_2$	LIPON	Cu	4.2–3.5	1–5	130 $\mu Ah\,cm^{-2}$	[29]	t26.9
$LiCoO_2$	LIPON	Li	4.2–2.0	50–400	35 $\mu Ah\,cm^{-2}$	[28]	t26.10
$LiMn_2O_4$	LIPON	Li	4–5.3	10	10–30 $\mu Ah\,cm^{-2}$	[37]	t26.11
Li-V_2O_5	LIPON	Li	1.5–3	2–40	10–20 $\mu Ah\,cm^{-2}$	[38]	t26.12
$LiCoO_2$	LIPON	SiSnON	2.7–4.2	~5,000	340–450 $mAh\,g^{-1}$	[39]	t26.13
$LiMn_2O_4$	LIPON	Li	4.3–3.7	~800	45 μ Ah ($cm^{-2}-\mu m^{-1}$)	[30]	t26.14
$LiCoO_2$	$Li_{6.1}V_{0.61}Si_{0.39}O_{5.36}$	SnO	2.7–1.5	10–200	4–10 $\mu Ah\,cm^{-2}$	[40]	t26.15

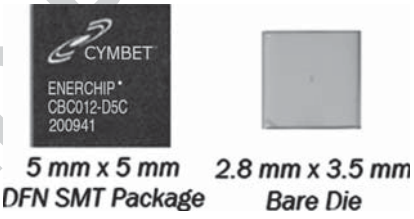

Fig. 20.4 Thin-film battery CBC012 marketed by Cymbet, at right with encapsulation of integration with other integrated circuits [14]

Table 20.4 Technical specifications of marked Cymbet batteries

Technical aspects	CBC012	CBC050	CBC3112	CBC3150	t27.1
Output voltage (V)	3.8	3.8	3.3	3.3	t27.2
Capacity (μAh)	12	50	12	50	t27.3
Charge time (min)	30	50	30	50	t27.4
Charge/discharge cycles	>5,000	>5,000	>5,000	>5,000	t27.5

- CBC012 (5 mm by 5 mm with a thickness of 0.9 mm) 249
- CBC050 (8 mm by 8 mm with a thickness of 0.9 mm) 250
- CBC3112 (7 mm by 7 mm with a thickness of 0.9 mm) 251
- CBC3150 (9 mm by 9 mm with a thickness of 0.9 mm) 252

The models CBC012 and CBC050 are also available with a package that allows 253
connection to other integrated circuits (Fig. 20.4). CBC31xx models already include 254
a load control and the ability to adjust to the output voltage. Its technical characteris- 255
tics can be found in Table 20.4. The Cymbet in conjunction with Texas Instruments 256
also offers systems consisting of thin-film batteries and energy harvesting tech- 257
niques. 258

Infinite Power Solutions also sells thin-film battery using $LiCoO_2$ as the cathode, 259
the LIPON as electrolyte, and metallic lithium as the anode. This provides, like 260
Cymbet, four models of thin-film batteries. Its technical characteristics can be found 261
in Table 20.5. 262

Table 20.5 Technical specifications of marked Infinite Power Solutions batteries

Technical aspects	MEC125	MEC120	MEC101	MEC102	t28.1
Open voltage(V)	4.1	4.1	4.1	4.1	t28.2
Internal resistance (Ω)	200	100	35	15	t28.3
Capacity (mAh)	0.2	0.4	1	2.5	t28.4
Charge time up to 90% (min)	15	15	15	15	t28.5
Life cycle (years)	>15	>15	>15	>15	t28.6
Charge/discharge cycles	>10,000	>10,000	>10,000	>10,000	t28.7
Self-discharge by year	<1%	<1%	<1%	<1%	t28.8

20.2.3 Materials for Lithium Batteries 263

Due to its characteristics, lithium is one of the most common materials used in solid-state batteries [21]. Lithium batteries are usually categorized by the anode material. Thus, batteries with metallic lithium anode are commonly known as "Li-Batteries". Batteries with anode of metal oxide or nitride are commonly known as "Li-ion Batteries" and batteries where the anode is also the current collector, usually copper, "Li-free Batteries." 264 265 266 267 268 269

In lithium batteries, the operating voltage is only defined by the chemical composition of the battery cathode and anode and not by its size. Rather, the capacity is defined by the volume of the battery cathode and anode. More volume means greater amount of lithium atoms, which results in a higher charge. During battery discharge, the operating voltage can go down a bit due to the battery's internal resistance. 270 271 272 273 274 275

Figure 20.5 illustrates the discharge of a rechargeable battery with a cathode of lithium cobalt oxide ($LiCoO_2$) and lithium metallic anode. In the battery charge process is carried out the extraction of about 50% of lithium from the cathode, which will be transferred to the anode. The lithium transferred will be used later in the discharge. However, considering the lithium anode, an even higher percentage of lithium will be transferred in the discharge. Chemical reactions of charge/discharge are shown in Table 20.6. 276 277 278 279 280 281 282

The separation between the battery cathode and anode is obtained through the electrolyte, which allows the passage of lithium ions, without letting pass lithium atoms or free electrons. Current collectors of the cathode and anode only allow the passage of electrons. When an external circuit is connected to the battery, an oxidation reaction occurs at the battery anode. This reaction will stimulate the electrons, through the external circuit, and the ions, through the electrolyte, to flow to the battery cathode. The lithium ions move into the gaps created in the cathode during battery charge. The electrons and ions will recombine again in the battery cathode [4]. 283 284 285 286 287 288 289 290 291

In Li-ion batteries the materials normally used as anode are SnO_2, $LiNiO_2$, $LiMn_2O_4$, V_2O_5, MoS_2, TiS_2 among others [42]. These materials must have the ability to accept large amounts of lithium ions. After battery fabrication the anode with these materials may not contain lithium, which restricts the choice of a 292 293 294 295

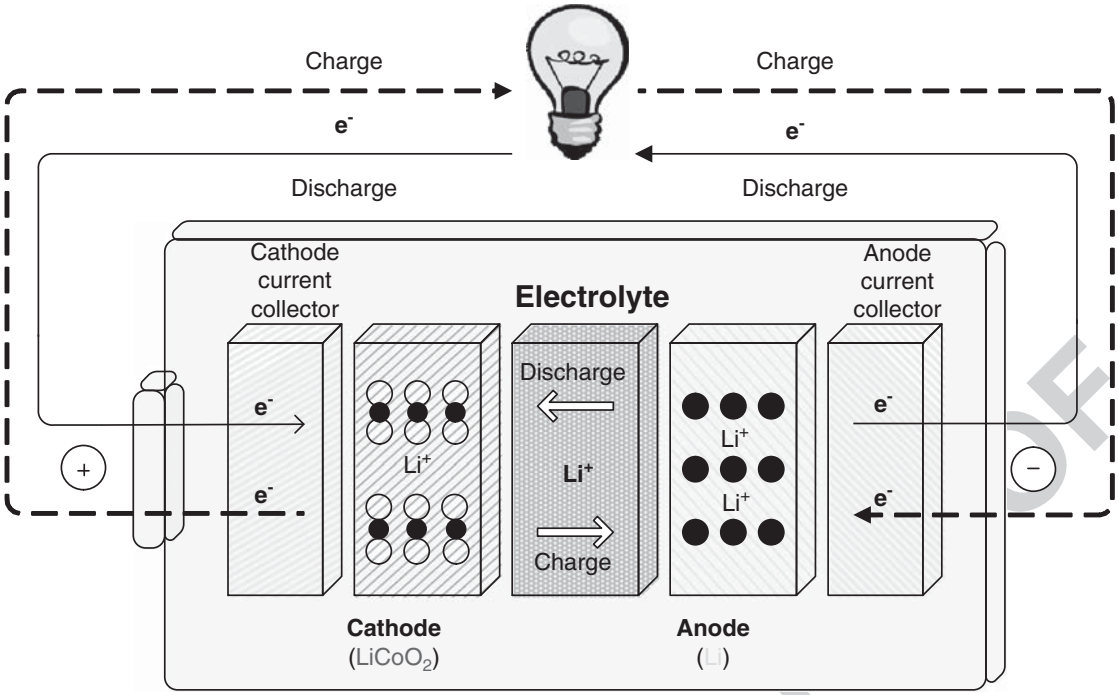

Fig. 20.5 Rechargeable lithium battery with $LiCoO_2$ cathode, where the empty circles represent the cobalt and oxygen atoms and the full circles the lithium atoms

Table 20.6 Chemical reactions of charge/discharge in a rechargeable lithium battery

Rechargeable lithium battery		
Charge	$LiCoO_2 = 0.5Li + Li_{0.5}CoO_2$	t29.1
Discharge	$0.5Li + Li_{0.5}CoO_2 = LiCoO_2$	t29.2

cathode in a lithium-rich cathode, the $LiCoO_2$, the $LiMn_2O_4$ and the $LiNiO_2$ being the most common.

The battery capacity or the amount of charges that can be provided are expressed in the amount of flowing current in a period of time (in hours), with the units Ah. $1\,A = 1\,C\,s^{-1}$, the battery capacity can also be expressed in Colombo (C), where 1Ah corresponds to 3600 C.

The battery energy is given by its operating voltage multiplied by the loads supplied and is usually expressed in Wh. For example, a battery with an operating voltage of 4.2 V and a capacity of 50 μ Ah, provides an energy of 210 μ Wh. Contrary to the operating voltage, the battery energy depends on its size, since the amount of charge delivered is proportional to the cathode mass. The battery power supplied is its energy per unit time.

The energy and power per unit of volume or per unit of mass are often used to compare different battery technologies [21]. Figure 20.6 compares lithium thin-film batteries, lithium polymer batteries, and conventional batteries.

The battery's volumetric energy density is calculated by dividing the power supplied to a specific discharge rate by the total volume in liters, with the units $Wh\,L^{-1}$. The battery's gravimetric energy density is calculated by dividing the

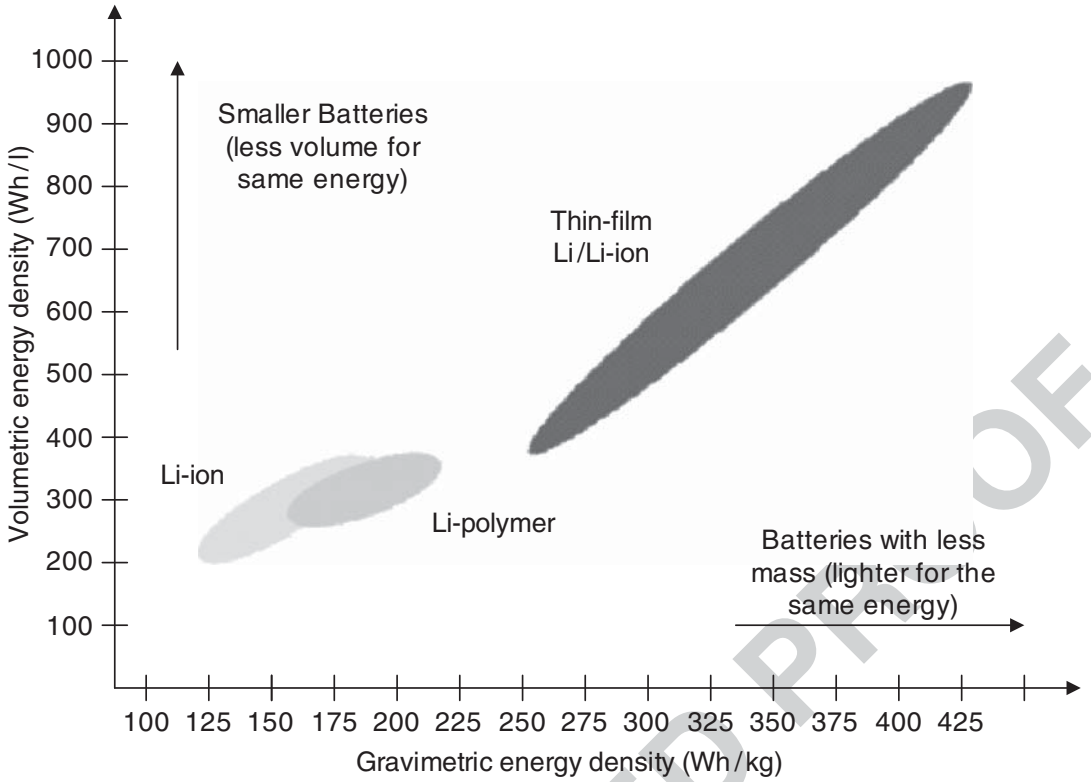

Fig. 20.6 Batteries – comparison of volumetric and gravimetric energy density [21]

power supplied to a specific discharge rate, by the total mass in kilograms, with the units $Wh\,kg^{-1}$. 314 315

The quality of a lithium ion battery's electrodes is very important to its energy density [21]. The most important characteristics of an electrode in a lithium-ion battery, which determine the energy that a battery can provide, are the number of electrons that the electrodes can store per unit volume or weight (volumetric and gravimetric energy density) and the electrochemical potential they produce. 316 317 318 319 320

20.2.3.1 Anodes 321

The anode is the ion source of battery [2]. The oxidation reaction occurs in the anode, ions and electrons being released into the electrolyte and the external circuit, respectively. Ions supplied by anode diffuse into the electrolyte. The anode should be a light metal or light metal compound with low electronegativity (tendency of an atom to attract electrons in a chemical bond) and high electrical conductivity. 322 323 324 325 326 327

Lithium is an excellent choice as the anode of a battery due to its low molecular weight and low electronegativity [42]. The lithium metal, although the most common material in the anodes of solid-state batteries, has a melting temperature of 180.7°C and is highly reactive with air. These reasons raise security issues in 328 329 330 331

Table 20.7 Anode material comparison [2]

Material (anode)	Capacity (mAh g^{-1})	Problem	t30.1
$Li_{21}Si_5$	1,967	Volume change after first charge/discharge cycle	t30.2
$Li_{22}Sn_5$	710	Volume change after first charge/discharge cycle	t30.3
LiC_6	370	Limited capacity	t30.4
InSb	270	Limited capacity	t30.5
$CaSi_2$	320	Limited capacity	t30.6
$Li_4Ti_5O_{12}$	168	Limited capacity	t30.7
SiTON	450	Loss capacity after first charge/discharge cycle	t30.8
SnO	1,560	Loss capacity after first charge/discharge cycle	t30.9

Table 20.8 Cathode material comparison [2]

Material (cathode)	Theoretical gravimetric energy density (Wh kg^{-1})	Open voltage in relation to metallic lithium (V)	t31.1
TiS_2	473	2.1–2.5	t31.2
V_2O_5	442	3–3.7	t31.3
$LiCoO_2$	500	3.6–4.7	t31.4
$LiMn_2O_4$	462	3–4.5	t31.5

a battery. Table 20.7 compares other possible materials for the battery's anode in relation to capacity and present the major problems.

The materials for the anode shown in table above were investigated. These materials cannot yet compete with lithium owing to reduced capacity, changes in materials' volume, and high capacity loss after the first charge/discharge cycle.

20.2.3.2 Cathodes

The cathode of a lithium battery is where reduction reaction occurs by electron transfer [2]. During the battery discharge, electrons and ions are transferred from the anode to the cathode. To enable a rapid and effective transfer, the cathode must have a high electrical conductivity, high diffusivity, and ion insertion capacity [42]. The higher the open voltage of the cathode in relation to a reference, the higher the operating voltage of the battery. The reference in lithium batteries is typically lithium metal. Table 20.8 compares some of the materials used as cathodes in lithium batteries, in relation to the theoretical gravimetric energy density and open voltage of metallic lithium.

The preceding table indicates that the $LiCoO_2$ is the material that has better characteristics, both in gravimetric energy density or the voltage level. The $LiMn_2O_4$ also shows high gravimetric energy and voltage level, while the TiS_2 and V_2O_5 present with features considerably lower than others.

Table 20.9 Electrolyte material comparison [2]

Material (electrolyte)	Electrolyte type	Ionic conductivity (Sc m^{-1})	t32.1
$LiClO_4$ or $LiPF_6$ in EC-DEC/DMC and PC	Liquid	10^{-3}–10^{-2}	t32.2
LiI	Solid	$\sim 5.5 \times 10^{-7}$	t32.3
$Li_{0,33}La_{0,56}TiO_3$	Solid	10^{-4}	t32.4
B_2O_3-$x$$Li_2O$-$y$$Li_2SO_4$ ($x < 0.6$ and $y < 0.3$)	Glassy	10^{-8}	t32.5
$x$$Li_2O$-$y$$SiO_2$-$z$$P_2O_5$	Glassy	10^{-9}–10^{-7}	t32.6
LIPON	Glassy	10^{-7}–10^{-6}	t32.7

20.2.3.3 Electrolytes 351

The electrolyte of a battery is essentially a passage for ions and a barrier to electrons or atoms without charge. Fundamental characteristics of an excellent electrolyte are a high ionic conductivity, high electrical resistivity, an excellent contact with the electrodes, and an excellent chemical stability in contact with the electrodes [2]. 352 353 354 355 356

In conventional batteries, the electrolyte is usually a liquid or an alkaline solution. This type of electrolyte, although it has high ionic conductivity, high electrical resistivity, and an excellent contact with the cathode, requires an airtight and heavy package, which reduces the energy density and increases the battery size [21]. To reduce the size and increase the energy density of a battery, a solid and glassy electrolyte is under investigation since 1970 [42]. Table 20.9 compares electrolyte materials in relation to their type and ionic conductivity. 357 358 359 360 361 362 363

The preceding table indicates less ionic conductivity of the glassy electrolyte than other types of electrolytes. However, the glassy electrolytes are still quite advantageous in battery safety. 364 365 366

Polymer electrolytes (PEs) are complexes formed between ionic salts and polymers with electron-donor atoms, such as linear high molecular weight poly (oxyethylene) (PEO). These materials are in general divided into two groups: solid (or solvent-free) PEs (designated as SPEs) and gel polymer electrolytes [43]. 367 368 369 370

SPEs were first introduced by Armand et al. [44] as an attractive alternative to non-aqueous liquid electrolytes in light-weight, rechargeable lithium batteries. The advantages of these materials include good electrochemical properties, a reduction in problems related to safety and environmental issues, and elimination of electrolyte leakage problems. These electrolytes may assume a multifunctional role as separator, adhesive, and cell sealant in electrochemical devices. Li^+-based SPEs are considered to be attractive materials for application in electrochemical devices such as galvanic cells, electrochromic displays, and sensors [45]. 371 372 373 374 375 376 377 378

The most studied solid-state polymer electrolyte (SPE) systems are based on poly(ethylene oxide), PEO, and are prepared by the dissolution of various guest ionic salts in the polymeric host matrix [46–50]. 379 380 381

In spite of their technological potential, SPEs suffer from a series of drawbacks that have delayed their application in lithium batteries. These include a marked tendency to crystallize, substantially lower ionic conductivity (typically 10^{-8} to $10^{-5}\,S\,cm^{-1}$ at room temperature) than non-aqueous liquid electrolytes and a tendency for the ionic guest species to salt out at high salt concentration. As liquid electrolytes also pose significant safety and environmental concerns, in recent years considerable effort have been devoted to increasing the ionic conductivity and improving the mechanical properties of SPEs [43].

Unfortunately, the rather modest ionic conductivity of known systems continues to restrict the application of these materials as components in commercial products. To increase conductivity, different polymer matrix architectures [51], liquid plasticizing components [52, 53], ceramic fillers [54], plasticizing salts [55], as well as ionic liquids have been evaluated [56].

The most extensively investigated PEO-based systems have included lithium salts [45] because of the applications in advanced primary and secondary batteries that can be foreseen.

Lithium bis(trifluoromethanesulfone)imide ($LiN(SO_2CF_3)_2$, LiTFSI)-based PE systems [57–61] give on the average higher conductivities than other lithium salts [62]. This improvement of ionic conductivity is attributed to the low lattice energy of the salt, which facilitates the solvation of the lithium by the polymer, and to the deslocalized negative charge on the nitrogen and four oxygen atoms, which reduces ion pairing tendency. In addition, because of its shape and internal flexibility, the TFSI-anion exerts a plasticizing effect and reduces the crystallinity of the PE, therefore lowering the glass transition of the materials.

Several recent papers by Zhang et al. [63–65] have demonstrated that lithium tetrafluoroborate ($LiBF_4$)-based electrolytes are a good alternative to lithium hexafluorophosphate ($LiPF_6$)-based materials as components in low temperature Li-ion batteries with improved performance. These authors found that, although an electrolyte based on a solution of $LiBF_4$ in propylene carbonate/ethylene carbonate/ethylmethyl carbonate had lower ionic conductivity and a higher freezing temperature than the $LiPF_6$-based analogue, at –20°C the $LiBF_4$-based cell had lower charge-transfer resistance than the $LiPF_6$-based device. In spite of the slightly lower conductivity of the $LiBF_4$-based electrolyte, the cell based on this system showed slightly lower polarization and higher capacity in the liquid temperature range (above –20°C) of the electrolyte. These results suggested that the ionic conductivity of the electrolytes is not necessarily a limitation to the low-temperature performance of the Li-ion cell. The $LiBF_4$ salt may be a good choice for a low temperature electrolyte of a Li-ion cell if a solvent system that has low freezing temperature, high solubility toward $LiBF_4$, and good compatibility with a graphite anode can be formulated. Examples of SPEs doped with $LiBF_4$ and supporting acceptable levels of room temperature ionic conductivity have already been reported [66–70].

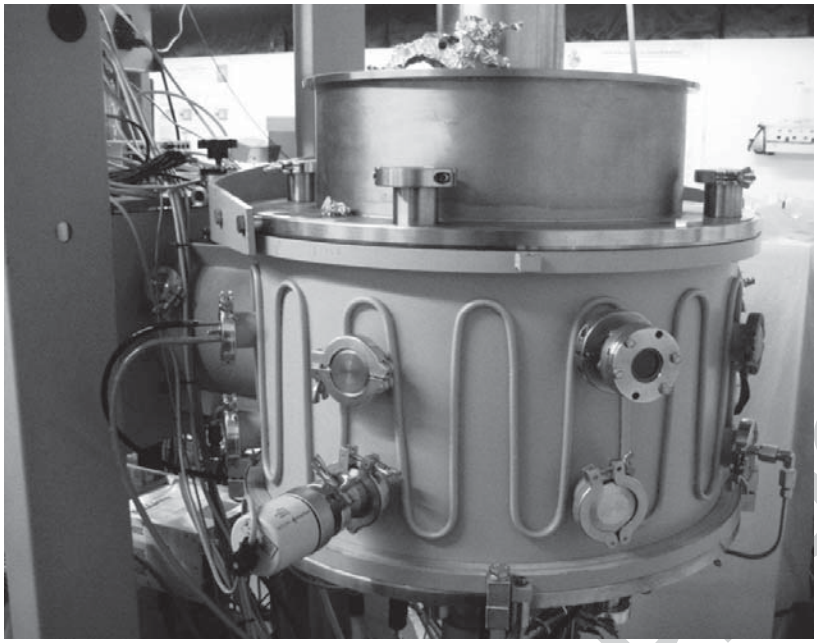

Fig. 20.7 Vacuum chamber for PVD depositions

20.3 Deposition and Characterization Techniques 425

20.3.1 Thin-Film Deposition 426

The deposition of thin films for current collectors, cathode, anode, and electrolyte of a battery was performed with the follow techniques: 427 428

- Thermal evaporation for anode; 429
- E-beam for current collectors; 430
- RF-Sputtering for cathode and electrolyte. 431

These thin-film deposition techniques belong to the group denominated as Physical Vapor Deposition (PVD) [71]. The utilization of these techniques requires a controlled atmosphere as in vacuum chambers, like in Fig. 20.7. 432 433 434

20.3.1.1 Thermal Evaporation 435

The thermal evaporation technique consists of the evaporation or sublimation of a material owing to heating of the same [72]. When the material passes from the solid state to the vapor state, without becoming a liquid, sublimation occurs. The material creates vapors that after condensation in the substrate, forms a thin film of the same material. The heat is achieved by applying a high current to a crucible that contains the material that should evaporate (Fig. 20.8). The standard crucibles are in tungsten, molybdenum, or tantalum because they have high temperatures of 436 437 438 439 440 441 442

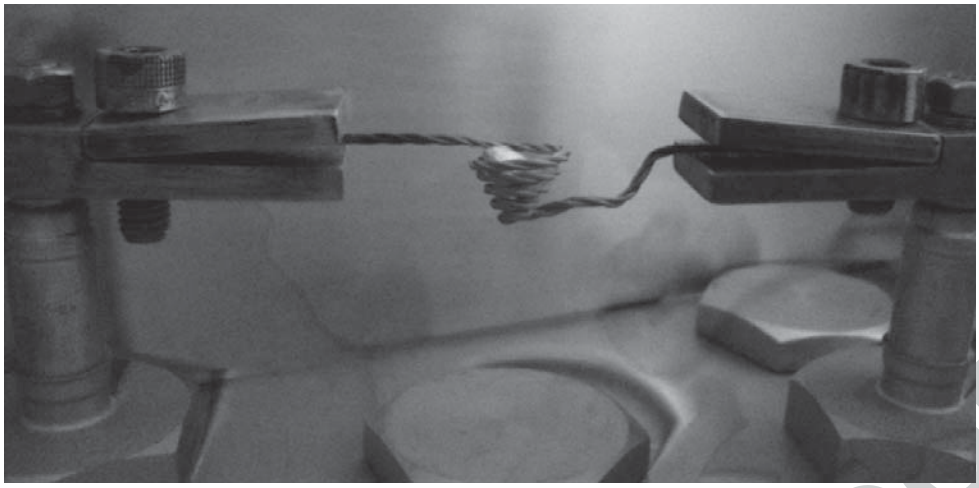

Fig. 20.8 Example of setup for thermal evaporation technique

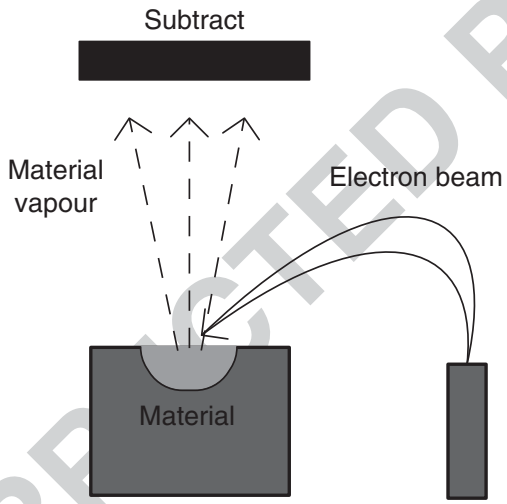

Fig. 20.9 Working demonstration of e-beam

evaporation/sublimation. The thermal evaporation technique is intended to create a thin film with the same composition of the material placed in the crucible [73].

20.3.1.2 Electron Beam

Like thermal evaporation, e-beam is also a technique to evaporate/sublimate a determinate material over a heater of the same. This technique uses a high energy beam of electrons that focuses on the material and will provide the heat (Fig. 20.9) [74]. A magnetic field helps to target the electron beams onto the material. The beams of electrons focus on a small area of material thus preventing contamination [73] in comparison with thermal evaporation because it is possible to reach higher temperatures. Figure 20.10 shows a setup for e-beam.

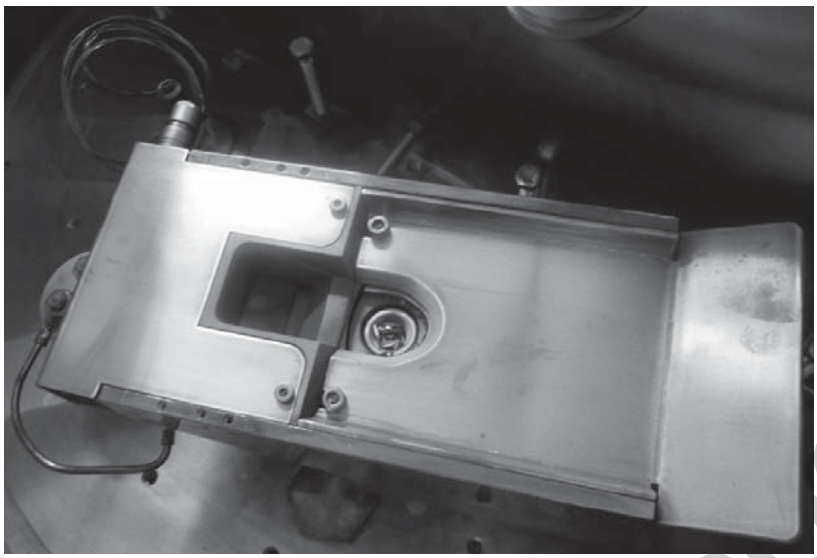

Fig. 20.10 Example of setup for e-beam

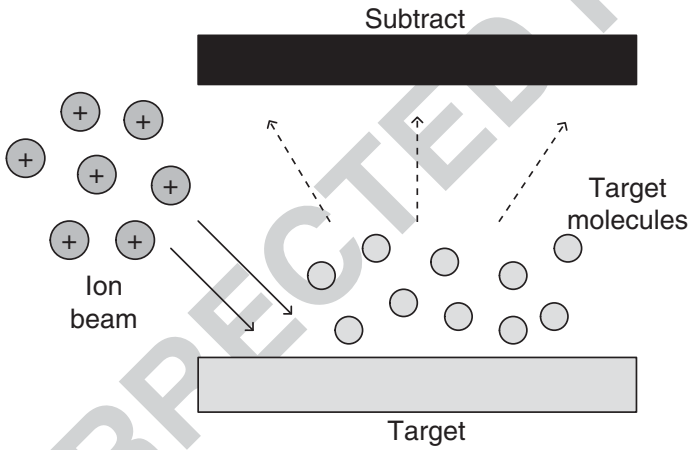

Fig. 20.11 Working demonstration of sputtering technique

20.3.1.3 Sputtering

The sputtering technique allows the deposition of thin films at low temperatures (typically less than 150°C) [73]. The material to be deposited, denominated of target, is bombed with a beam of positive ions, that forces the extraction of molecules/atoms at the target surface. The beam of ions is achieved by the ionization and acceleration of a gas (normally argon) inside the chamber [72]. The extracted molecules/atoms will form the thin film on the substrate (Fig. 20.11). The sputtering technique allows the deposition of thin films with better characteristics in terms of composition and uniformity [71], owing to a large area for the incidence of ion beams on the target.

The sputtering technique can be done by direct current (DC sputtering) or by radio frequency (RF sputtering). The DC sputtering is only applied to conductive

Fig. 20.12 Magnetron with Li_3PO_4 target

materials, while the RF sputtering does not have that restriction [71]. Figure 20.12 shows a magnetron with a Li_3PO_4 target (used in electrolyte deposition).

20.3.2 Material Characterization

The thin-film characterization is performed using X-Ray Diffraction (XRD), Energy-Dispersive X-ray-spectroscopy (EDX), and Scanning Electron Microscope (SEM) techniques.

20.3.2.1 X-Ray Diffraction

The XRD allows the quantification of crystalline structure of a given material. This technique is only possible because the atoms are usually ordered in crystal planes separated by distances of the same order of magnitude of the X-rays wavelength [75].

The phenomenon of diffraction occurs when an X-ray beam covers the crystal and interacts with the present atoms. The XRD is based on Bragg's Law (Equation 20.1) establishing the relationship between diffraction angle and the distance between the planes giving rise to (characteristic for each crystalline phase) [76].

$$n\gamma = 2d \sin\theta \tag{20.1}$$

Where:

- n is a whole number
- γ is the wavelength of incident X-rays
- d is the distance between the planes
- θ is the diffraction angle.

When compared with others, the XRD technique is simple, fast, and reliable. The possibility of analysis of materials composed of a mixture of phases and a quantitative analysis of these phases are the advantages of XRD.

20.3.2.2 Dispersive X-Rays Spectroscopy and Electronic Scan Microscopy

The EDX is an electron beam that focuses on a sample (which must be electrically conductive), causes excitation and removal of electrons from one orbit inside the material, creating a gap. The X-ray emission occurs when an electron from an outer orbit occupies the created gap. Chemical analysis of sample composition is possible because the wavelengths emitted are specific to each element of a material. The analysis is performed on all the material from the surface up to 2 μm depth and does not allow the composition of elements with a low atomic number (lithium for example).

The equipment composition by EDX analysis normally incorporates the SEM microscope. The SEM technique allows the achievement of an image of the surface material through the capture of electrons generated by a detection array [77].

20.3.3 Other Physical Measurements on Thin-Film Batteries

Apart from the traditional characterizations for thin films explained above, other physical measurements were performed, namely electrical resistivity, ionic conductivity, differential scanning calorimetry, thermal gravimetric analysis, and cyclic voltammetry.

20.3.3.1 Electrical Resistivity

The electrical resistivity was measured at four points (Fig. 20.13), using the Van der Pauw method [78].

The asymmetric configuration, the geometry of contact, and the material anisotropy are corrected by repeating the measurement in four different configurations (Fig. 20.14). This technique of measuring at four points requires uniformity in the thickness of the sample [72].

The voltage drop is measured between two points while a constant current intensity is applied at the other two points. The voltage and current values are then used in Equations 20.2 and 20.3, to calculate R_A and R_B, respectively.

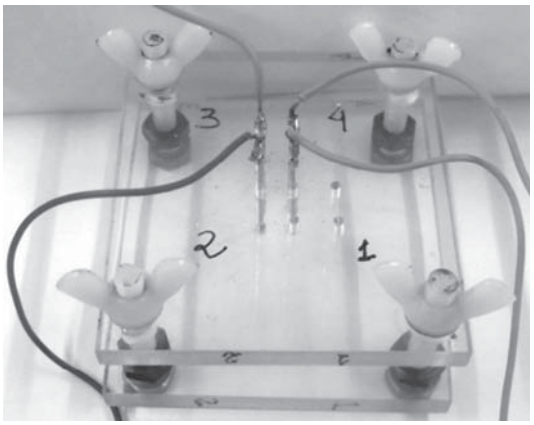

Fig. 20.13 Setup for measuring resistivity

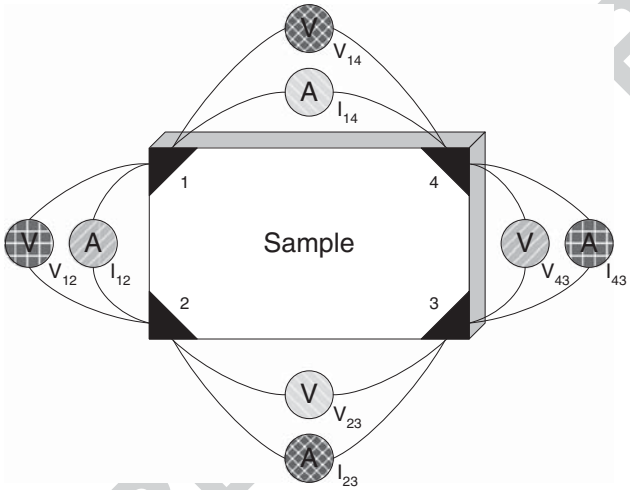

Fig. 20.14 Schematic of each measure needed for the resistivity measurement

$$R_A = \frac{V_{12}}{2I_{43}} + \frac{V_{43}}{2I_{12}} \tag{20.2}$$

$$R_B = \frac{V_{14}}{2I_{23}} + \frac{V_{23}}{2I_{14}} \tag{20.3}$$

Knowing R_A and R_B, and using the Equation 20.4, the value of R_S is calculated by numerical convergence.

$$e^{\left(-\pi \frac{R_A}{R_S}\right)} + e^{\left(-\pi \frac{R_B}{R_S}\right)} = 1 \tag{20.4}$$

The value of resistivity is finally calculated with the value of R_S and the film thickness (h), as shown in Equation 20.5.

$$\rho = R_S h \tag{20.5}$$

20.3.3.2 Ionic Conductivity

The ionic conductivity is an important characterization parameter, which has been used as the criterion for quantification of electrolyte quality in lithium batteries. The ionic conductivity is a measure of the amount of ions or ion clusters that can move through the action of an electrical or chemical potential [79]. In general, the ionic conductivity of the electrolytes is measured as a function of salt composition and temperature. The objective of this characterization is to identify the electrolyte with the most favorable behavior for use as a component of the practical device.

Lithium batteries can have two different types of electrolytes. The solid electrolytes, that allow the fabrication of all batteries by PVD techniques and the more common polymer electrolytes (PEs). A solid electrolyte and a PE intended for use in diverse electrochemical applications must have adequate ionic conductivity, together with negligible electronic conductivity if self-discharge on standing is to be avoided. A PE is considered to be a promising candidate for commercial application if its ionic conductivity is as high as 10^{-5} S cm^{-1} at room temperature [80–82].

In general, salts with a polarizing cation and a large anion with a well-delocalized charge, and therefore also with low lattice energy, are the most suitable for use as PEs [83, 84]. In spite of the dangers associated with the anion, lithium perchlorate ($LiClO_4$) is a salt that satisfies the conditions mentioned above. Lithium trifluoromethanesulfonate (or triflate) ($LiCF_3SO_3$) and lithium tetrafluoroborate ($LiBF_4$) have also been extensively employed in this context [85]. Lithium bis(trifluoromethanesulfonyl)imide (LiTFSI) is particularly interesting as a guest species in solid PEs and also one of the best choices. In common with other salts that contain large polarizable anions, LiTFSI has low lattice energy and a low tendency to form ion-pairs, leading to enhanced ionic mobility. This salt also performs as a plasticizer in polyether electrolytes by creating free-volume. This is a significant advantage in polymer hosts that have an inherent tendency to crystallize.

Typically the total ionic conductivity of the electrolytes discussed here was measured by placing the sample between gold blocking electrodes, along the so-called *electrode/electrolytes/electrode assembly* (Fig. 20.15), which was secured in a suitable constant-volume support, to form a symmetrical cell. Low-amplitude alternating potentials at frequencies between 65 kHz and 0.5 Hz were applied over a range of temperatures from 20°C to 80°C. This technique is possible, in an appropriate electrochemical system, owing to separation of the analysis of the electrolyte response and the connections electrode/electrolyte response (Fig. 20.16).

The electrodes are typically in the form of reduced thickness disk, minimizing the separation distance between the electrodes and maximizing the area. This also allows the decreasing of electrical current that goes through the system which seeks to eliminate the possible change of electrochemical properties of the sample. These conditions guarantee that no transfer of electrical charge through the metal/electrolyte interface happens, because these interfaces exhibit a purely capacitive behavior. Whereas the electrode/electrolyte interfaces are equal, the equivalent circuit of Fig. 20.17 can be considered [86]. So for high frequencies, the impedance is dominated by the parallel circuit, corresponding to the electrolyte. For low

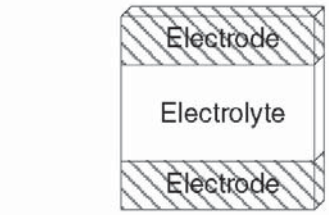

Fig. 20.15 Sample for ionic conductivity measure

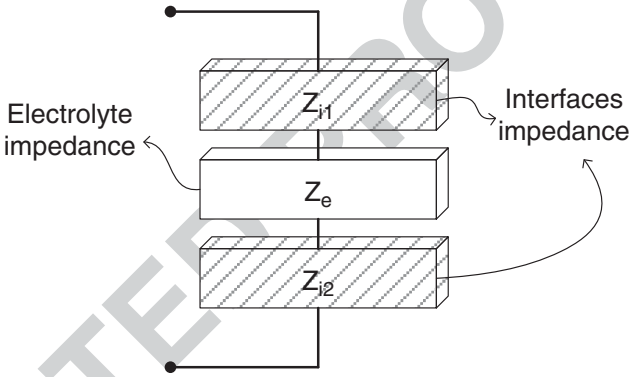

Fig. 20.16 Impedance of samples for ionic conductivity measurement [79]

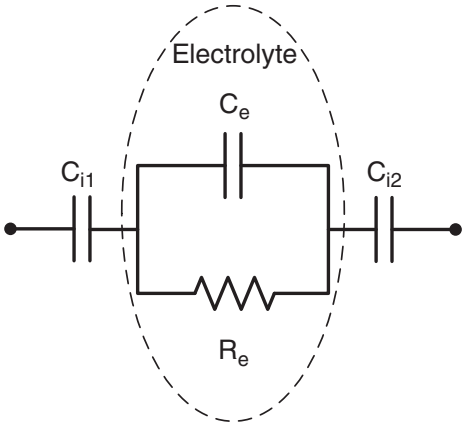

Fig. 20.17 Equivalent circuit of sample for ionic conductivity measurement [79]

frequencies, the impedance is dominated by the series circuit, predominantly electrode/electrolyte interfaces [87].

The frequency spectrum is studied through the Nyquist diagram of the sample impedance. The Nyquist diagram is accomplished by applying a sinusoidal voltage to the sample in a high frequency range. Figure 20.18 shows an example of a Nyquist diagram obtained with this technique. The figure shows that after tracing the Nyquist diagram, it is necessary to draw a semicircle to get the value $R(\Omega)$.

The R value is then applied in Equation 20.6, h being the film thickness, A the area and ρ the ionic conductivity.

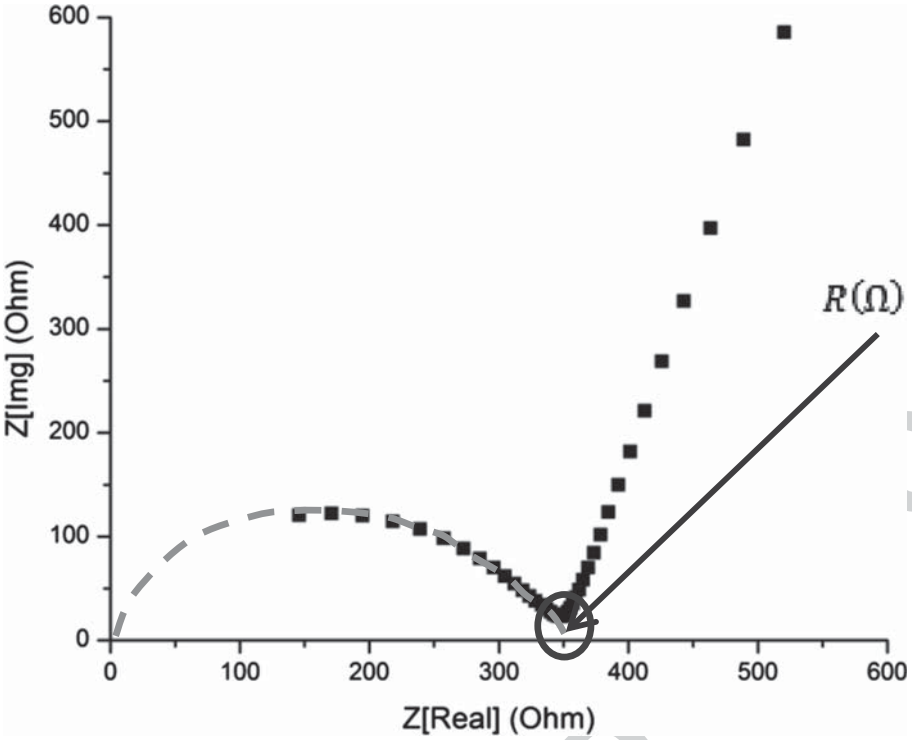

Fig. 20.18 Example of a Nyquist diagram from an electrolyte sample

$$\rho(\mathrm{Sc\,cm^{-1}}) = \frac{h(\mu\mathrm{m})}{R(\Omega) \times A(\mathrm{cm^2}) \times 10,000} \tag{20.6}$$

20.3.3.3 Thermal Properties

Thermal analysis techniques, in particular Differential Scanning Calorimetry (DSC) and Thermogravimetric Analysis (TGA), are valuable tools to study the thermal behavior of electrolytes.

Differential Scanning Calorimetry

The DSC is a technique of differential thermal analysis based on the release or absorption (depending on the material) of heat by the sample [88]. This technique characterizes the sample through the temperature difference between the sample itself and a reference material. Figure 20.19 represents a schematic illustration of DSC where one can see that the heating elements and temperature sensors of the sample and the reference are independent. The reference material is chosen to be inert and not subject to the release or absorption of heat in the temperature range investigated. This technique requires a chamber with controlled temperature and atmosphere. The atmosphere in the chamber is controlled by introducing an inert gas to clean the chamber prior to measurement, to protect the sample, and to prevent the deposition of ice on the inner surfaces of the chamber when operating at negative temperatures.

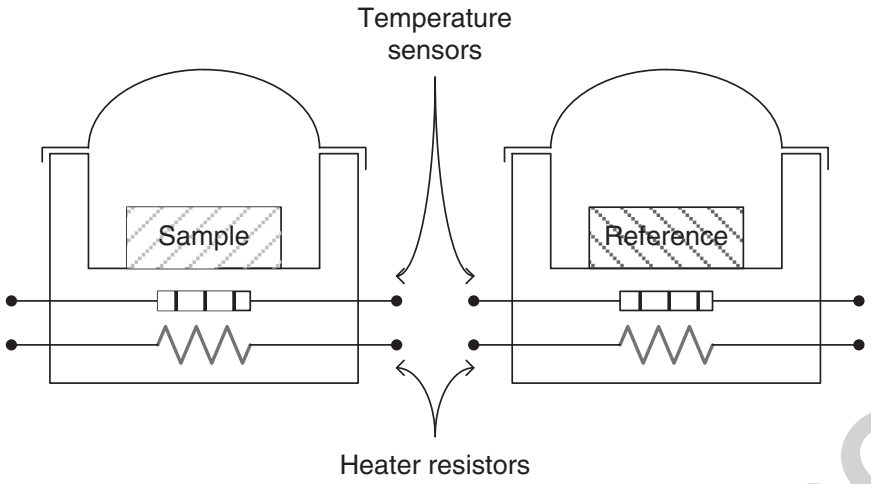

Fig. 20.19 Schematic representation of DSC

In case of PEs, DSC allows to calculate the proportion of crystallinity, detect the formation of new crystalline phases, free guest salt or uncomplexed polymer chains, monitor the loss of solvent(s) (e.g., occluded water, alcohol), determine the T_g value, and distinguish between endo- and exothermic events. For the DSC measurements of PE samples, sections are usually subjected to thermal analysis under a flowing inert atmosphere between 25°C and 300°C and at a heating rate of 5°C min^{-1}.

Given the relative simplicity of construction, convenience in use, and adequate precision for most applications, DSC is the preferred choice of manufacturers and the more common thermal analysis technique.

Thermal Gravimetric Analysis

The thermal analysis techniques are usually a group of techniques that registers a particular property of the sample as a function of temperature. In the TGA technique the weight of the sample as a function of temperature is registered. The realization of this technique is based on the use of a thermal balance and requires a chamber with controlled temperature and atmosphere [88]. You need a prior knowledge of the mass of the sample at room temperature. The onset of thermal decomposition is estimated by extrapolation from the TGA curves (Fig. 20.20). TGA provides rich information about the thermal degradation of the samples and their thermal stability domain.

20.3.4 Cyclic Voltammetry

The application of the PEs in electrochemical applications depends on their stability window.

To evaluate the electrochemical stability window of PE compositions we have typically used a two-electrode cell configuration involving the use of a 25 μm-diameter gold microelectrode surface. Cell assembly was initiated by locating a

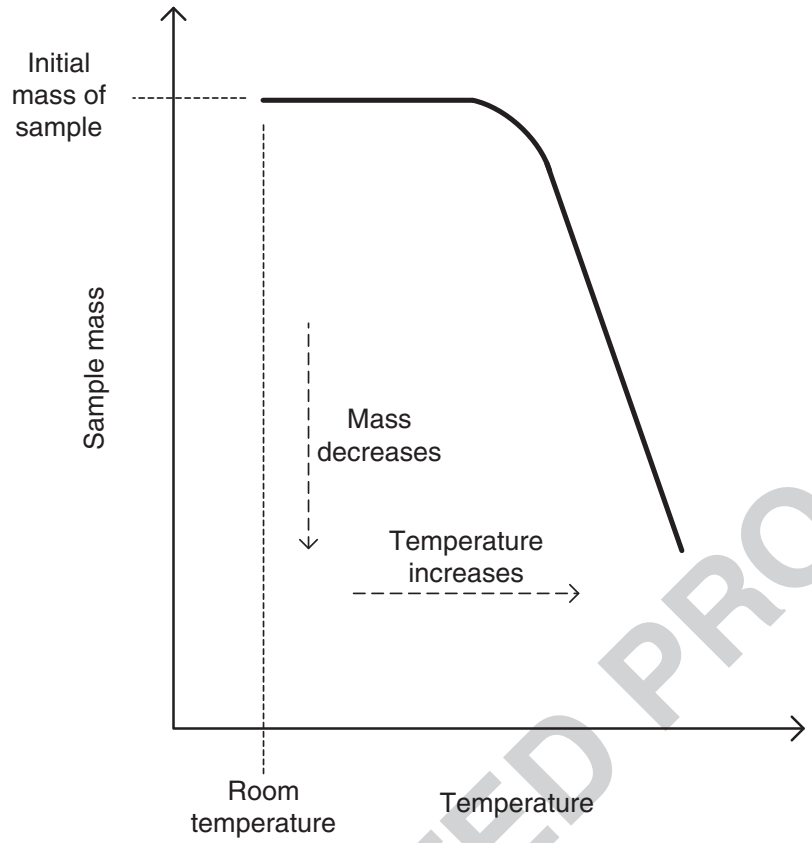

Fig. 20.20 Typical graph of TGA

freshly cleaned lithium disk counter electrode on a stainless steel current collector. A thin-film sample was centered over the counter electrode and the cell assembly completed by locating and supporting the microelectrode in the centre of the electrolyte disk. Measurements were conducted at room temperature within a Faraday cage.

The electrochemical stability range of the lithium-doped di-ureasils was determined by microelectrode cyclic voltammetry over the potential range between -1.5 and 6.5 V. In the anodic region, all electrolytes are stable up to 4.0 V *versus* Li/Li^+. Lithium deposition begins in the cathodic region at about -0.5 V *versus* Li/Li^+. These results suggest that the electrochemical stability of the PEs is acceptable for application in practical devices.

20.4 Fabrication and Characterization

20.4.1 Electrical Contacts

Platinum was the material chosen for the battery's contacts as having high electrical conductivity, being inert in contact with other battery materials, and allowing a better distribution of electrons at the cathode surface. The platinum was deposited

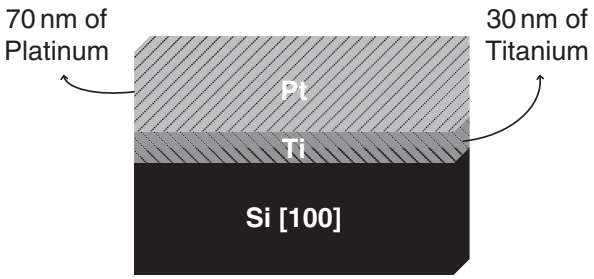

Fig. 20.21 Battery contacts depositions

by e-beam technique. The integration of the battery manufacturing processes with integrated circuits is a very important aspect and therefore, the substrate must be compatible with these requests. The chosen substrate was silicon because it is used the most in manufacturing processes of integrated circuits [71].

A deposition of 100 nm of platinum was taken up for adhesion investigation. It appears that the adhesion of platinum to silicon is very vulnerable and the films were shown to be damaged. The resolution of this problem was achieved with the prior deposition of 30 nm of titanium [89–91], also using the e-beam technique. This improved platinum adhesion and the films were not damaged. After depositing the two materials it is necessary to test their vulnerability to annealing, since this is necessary for the battery's cathode. The sample was placed in an oven for two hours in a vacuum at temperatures between 500°C and 800°C, that is, the same conditions necessary for the battery's cathode. Under these conditions of annealing, the films were not damaged, so the battery contacts are made of 30 nm of titanium and 70 nm of platinum (Fig. 20.21).

20.4.2 Cathode

Lithium cobalt oxide ($LiCoO_2$) was the chosen material for the positive electrode (cathode) of the thin-film solid-state battery. The $LiCoO_2$ was chosen because of its excellent electrochemical stability and its capacity for insertion and extraction of lithium ions. These characteristics derive from its excellent structural stability [92]. The most common material used in thin-film batteries is $LiCoO_2$, because it produces a high voltage [21, 93] and has a high performance over the cycles of charge/discharge (owing to its structural stability, it can hold more than 500 cycles of charge/discharge maintaining its capacity at about 80% to 90%). Compared with other materials (for example, $LiMn_2O_4$ and $LiNiO_2$), the $LiCoO_2$ is easy to fabricate and can store a large amount of lithium ions. $LiCoO_2$ was deposited by RF sputtering, and deposition parameters can be found in Table 20.10. Films were deposited with different gases to adjust to the fabrication process.

After his deposition, $LiCoO_2$ was subjected to annealing [94, 95]. The annealing increases the crystallization and decreases the resistivity of the $LiCoO_2$ film, being carried out at temperatures between 500°C and 800°C. $LiCoO_2$ films

Table 20.10 Cathode deposition parameters

Thin-film	Deposition technique	Target	Thickness	Pressure	Supply power	Gas (sccm)			t33.1 t33.2
						O_2	Ar	N_2	t33.3
#01	RF sputtering	$LiCoO_2$	1 μm	2×10^{-3} mbar	150 W	10	30	–	t33.4
#02						–	40	–	t33.5
#03						–	40	–	t33.6

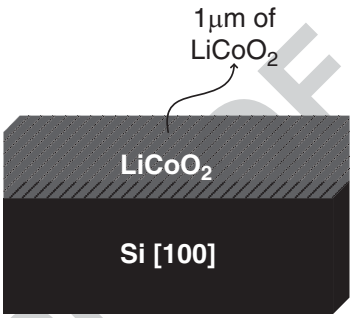

Fig. 20.22 Battery cathode illustration

annealing was performed in vacuum for two hours. Figure 20.22 illustrates the deposition of $LiCoO_2$ to proceed to the annealing after its characterization.

The thin-film characterizations were performed by XRD, Van de Pauw, EDX and SEM techniques to measure the crystallization, the electrical resistivity and chemical composition. Figure 20.23 shows the XRD patterns of $LiCoO_2$ films deposited for their annealing temperatures. Crystallographic analysis of the diffractograms was compared with the standard "016-0427" [96], which contains the crystal planes of $LiCoO_2$. In Fig. 20.23, the crystal planes are represented with red vertical lines. The spectra show the predominance of $LiCoO_2$ in the samples [97], especially in sample "#03" (sample with better features). A detailed analysis allows us to observe that the crystal planes of $LiCoO_2$ increases with increasing temperature to 700°C. The plan [003], in particular, is one which denotes this additional feature, being one of the most important [97]. The annealing at 650°C and 700°C proved to be most suitable for obtaining a $LiCoO_2$ film. The crystal structure of $LiCoO_2$ film increases the diffusivity of the lithium ion, which is a very important feature in the battery cathode.

The resistivity of $LiCoO_2$ films was measured by Van der Pauw technique. As can be seen in Fig. 20.24, the film subjected to an annealing of 650°C under the conditions described above, was the film with better resistivity, about 3.7 Ω-mm. The chemical composition of the film with improved resistivity was also analyzed by EDX in Fig. 20.25. Note that the atomic number of lithium is quite small, and therefore not covered by this technique. A SEM image was also performed (Fig. 20.26), which denotes the formation of crystals in the $LiCoO_2$ film surface.

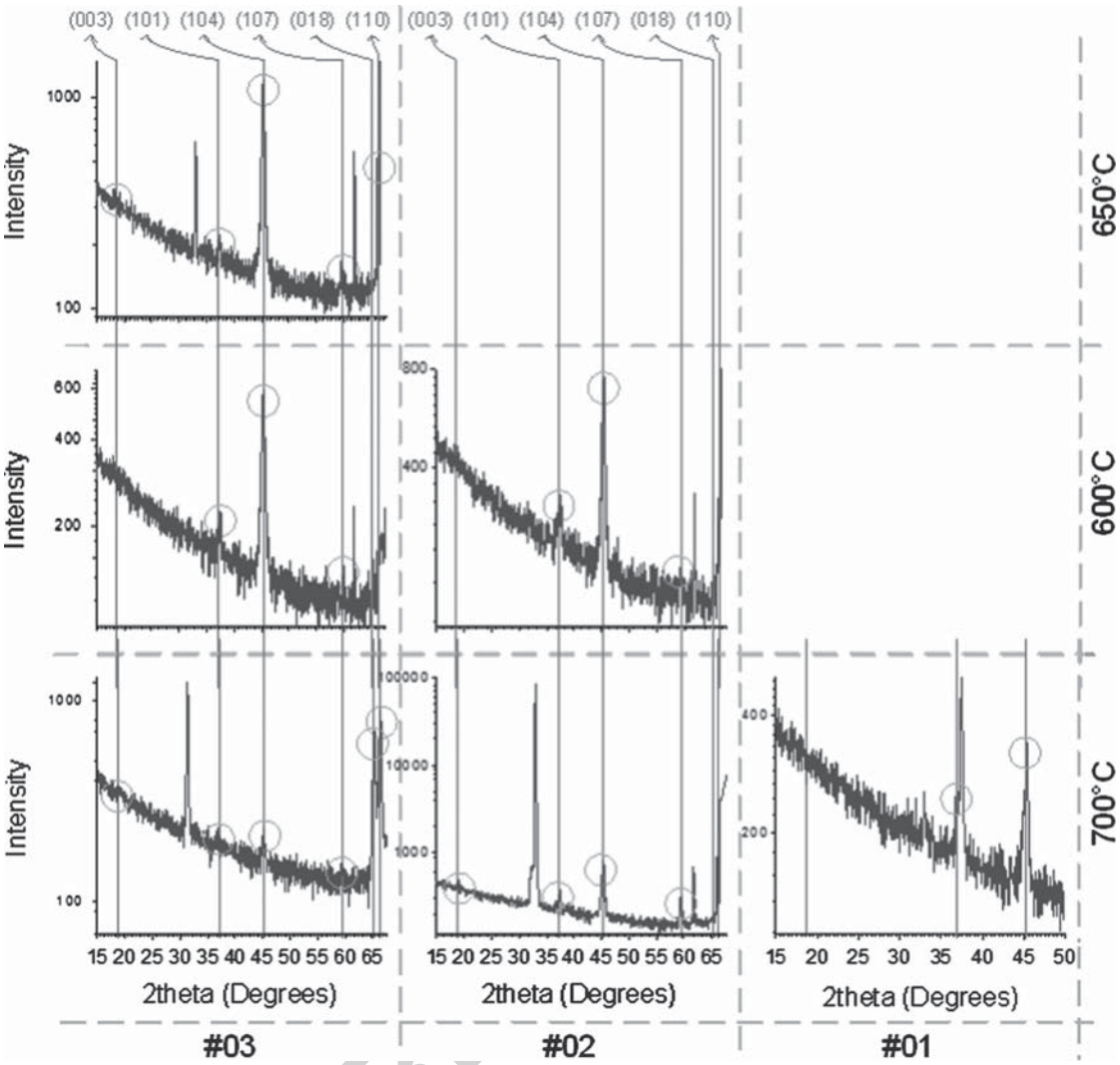

Fig. 20.23 XRD of $LiCoO_2$ films with annealing at 700°C, 600°C, and 650°C. Vertical lines (*red*) correspond to $LiCoO_2$ phases and circles (*green*) point to the correspondence phase in spectra

20.4.3 Electrolyte

The main features of the electrolyte are high ionic conductivity, high electrical resistivity, and stability when in contact with the cathode and anode of the battery [21]. It is generally accepted that amorphous materials (without crystal planes) have a higher ionic conductivity [98]. These characteristics are met by the lithium phosphorus oxynitride (LIPON), which is the chosen material for the electrolyte of thin-film solid-state batteries. The LIPON also has a high electrochemical stability, which drives its use in thin-film batteries [99]. An electrical resistivity greater than $10^{14}\Omega$-cm is also an important feature of LIPON, because it prevents the self-discharge of the battery, increasing the time it keeps the battery charged [100]. The LIPON was deposited by RF sputtering and the deposition parameters can be

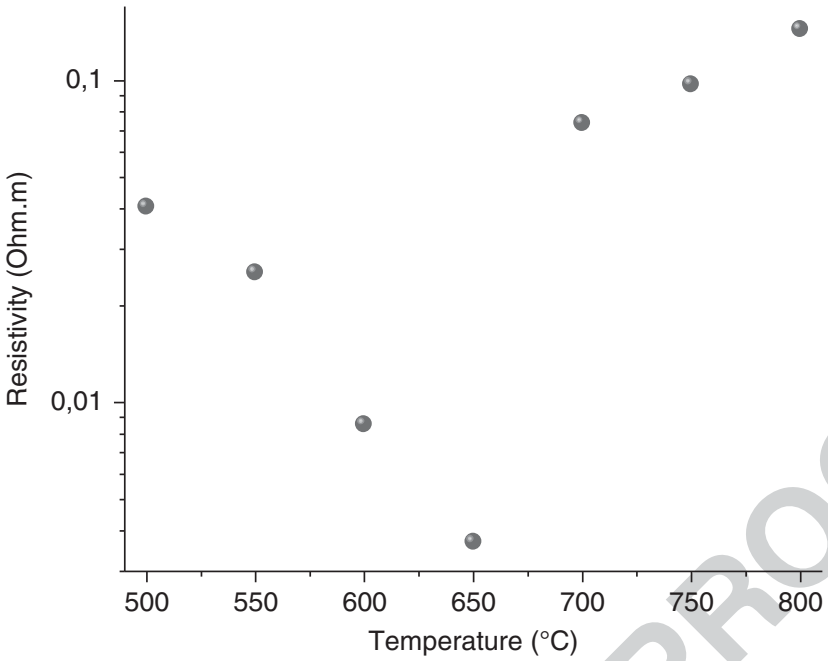

Fig. 20.24 $LiCoO_2$ films resistivity from deposition "#03"

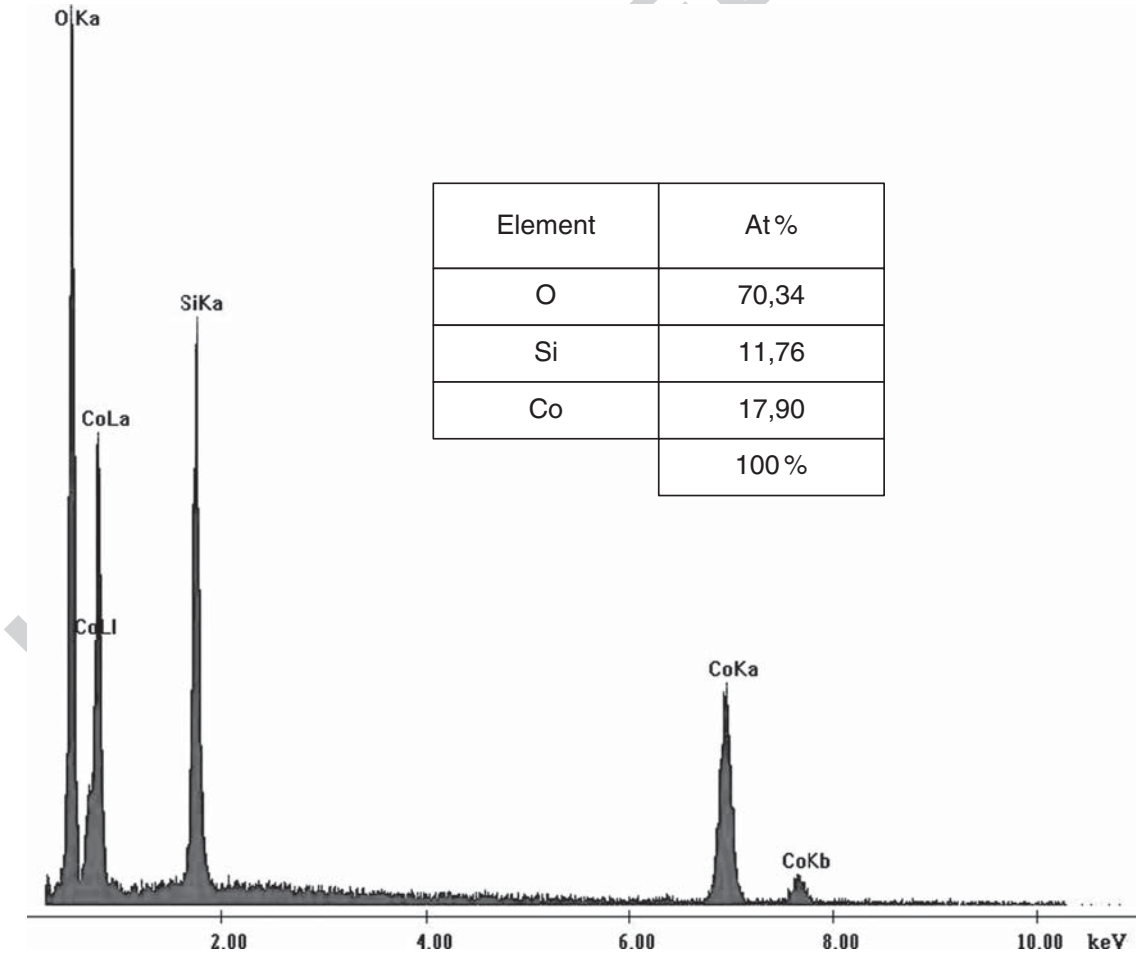

Element	At%
O	70,34
Si	11,76
Co	17,90
	100%

Fig. 20.25 $LiCoO_2$ film chemical composition

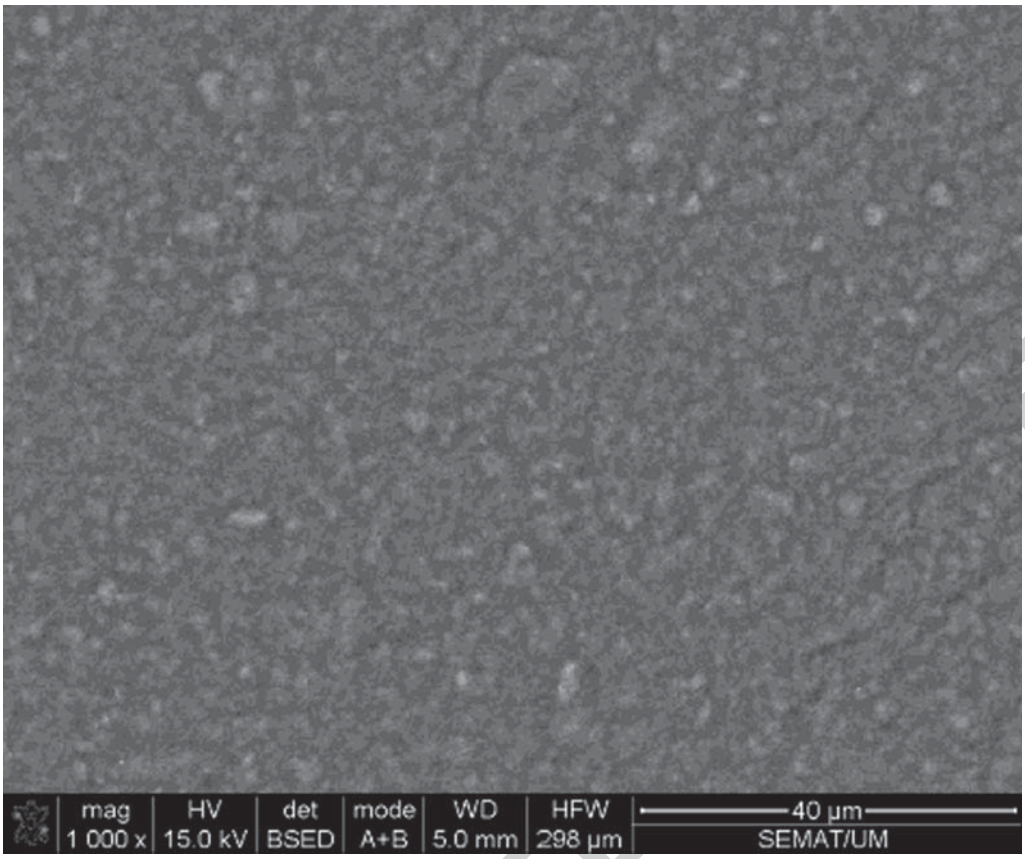

Fig. 20.26 $LiCoO_2$ film SEM, surface picture

Table 20.11 Electrolyte deposition parameters

Thin-film	Deposition technique	Target	N_2	Pressure (mbar)	Power supply (W)	Thickness	t34.1
#01	RF sputtering	Li_3PO_4	20 sccm	1×10^{-2}	200	1 µm	t34.2
#02				2×10^{-3}			t34.3
#03				7×10^{-3}			t34.4
#04				3×10^{-4}			t34.5
#05				3×10^{-4}	150		t34.6

found in Table 20.11. Pressure was kept at different values during the deposition of each film to correlate the deposition parameters with film properties.

Figure 20.27 illustrates the deposition of LIPON films to measure the ionic conductivity. The aluminum substrate was chosen because of its high electrical conductivity and low cost, being used as a contact. To improve contact, LIPON was deposited between platinum films. Subsequently, an aluminum disk with a diameter less than the substrate (to ensure non-occurrence of short circuit) was glued (using silver glue) at the top of the sample to ensure its robustness (Fig. 20.28).

The ionic conductivity was measured by applying a sinusoidal voltage with 25 mV peak to peak to the sample in a range of frequencies between 0.5 Hz and

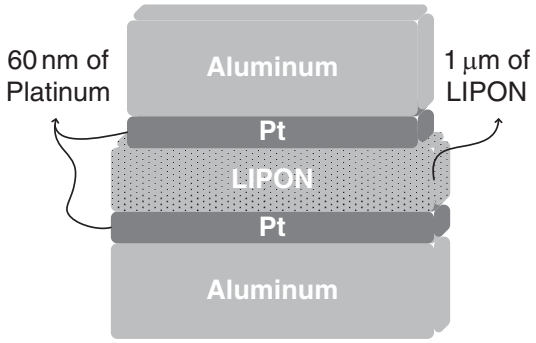

Fig. 20.27 Electrolyte deposition illustration

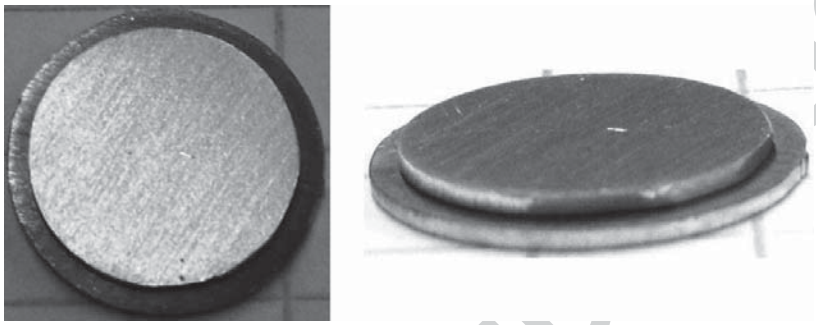

Fig. 20.28 LIPON sample with upper and lower contact

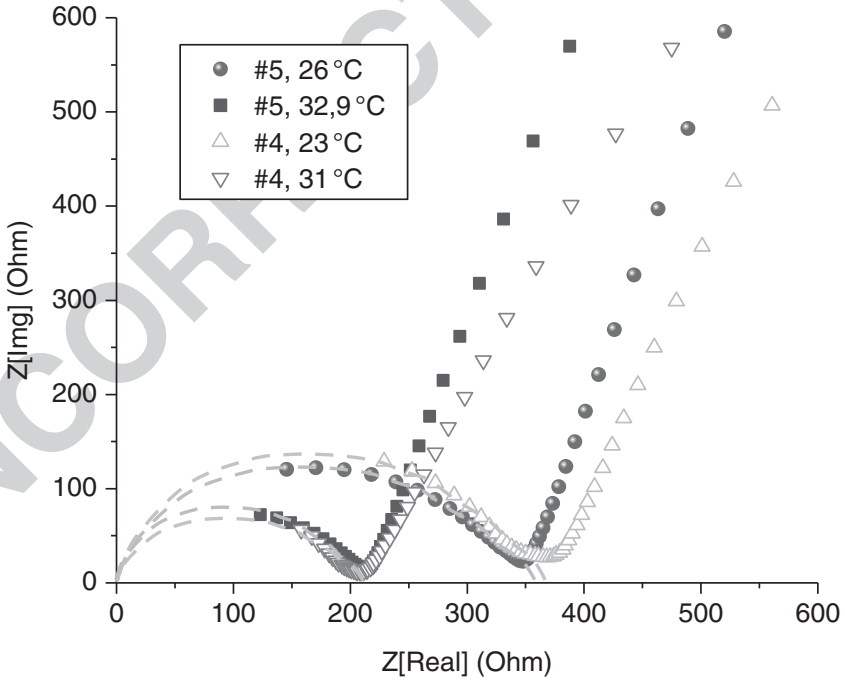

Fig. 20.29 Nyquist diagram of LIPON films

65 kHz. Reading the response of the sample allowed drawing of the Nyquist diagram of the sample impedance [98, 101]. Figure 20.29 gives examples of the Nyquist diagrams for samples "#4" and "#5" at different temperatures.

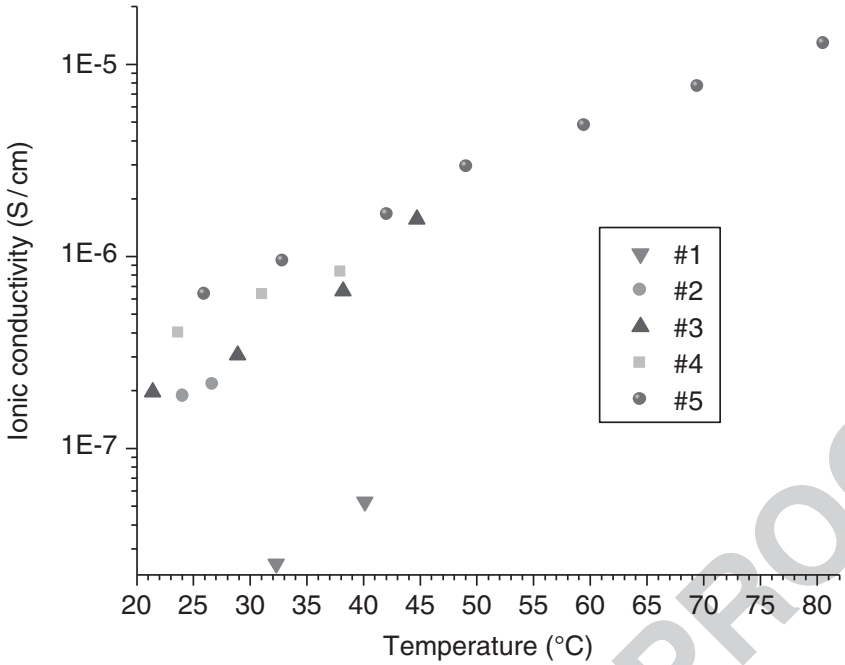

Fig. 20.30 Ionic conductivity of LIPON films

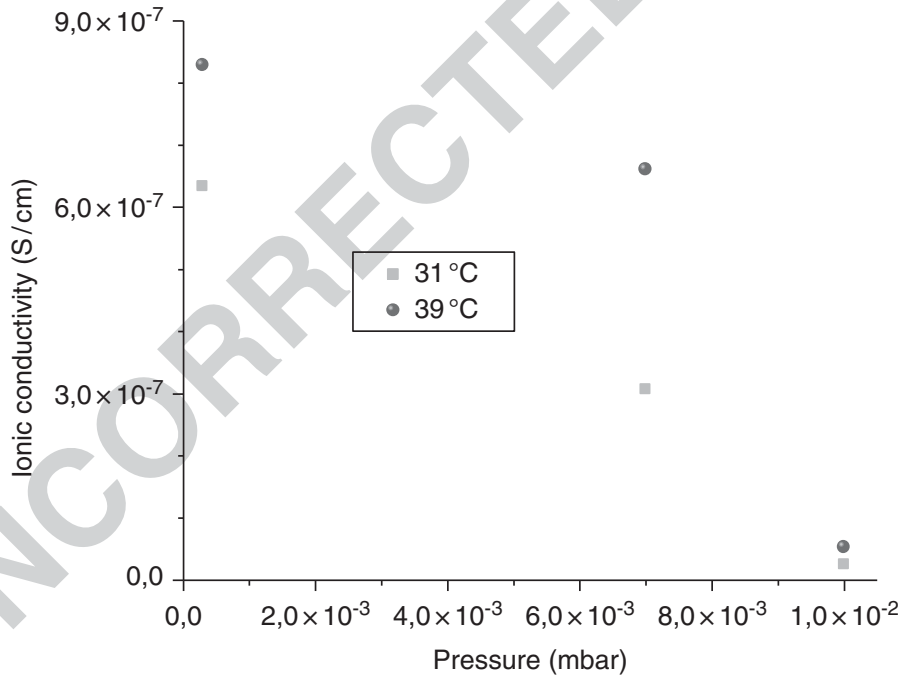

Fig. 20.31 Ionic conductivity of LIPON films as a function of pressure during deposition

Semicircles in the Nyquist diagram (Fig. 20.29) were traced with the help of a specific program (in this work Autolab was used). The intersection of the semicircle with the x-axis indicates the resistance value to be applied in the formula for ionic conductivity (Equation 20.6). Figure 20.30 shows the value of ionic conductivity for the various deposition parameters (Table 20.11). Please note that ionic conductivity

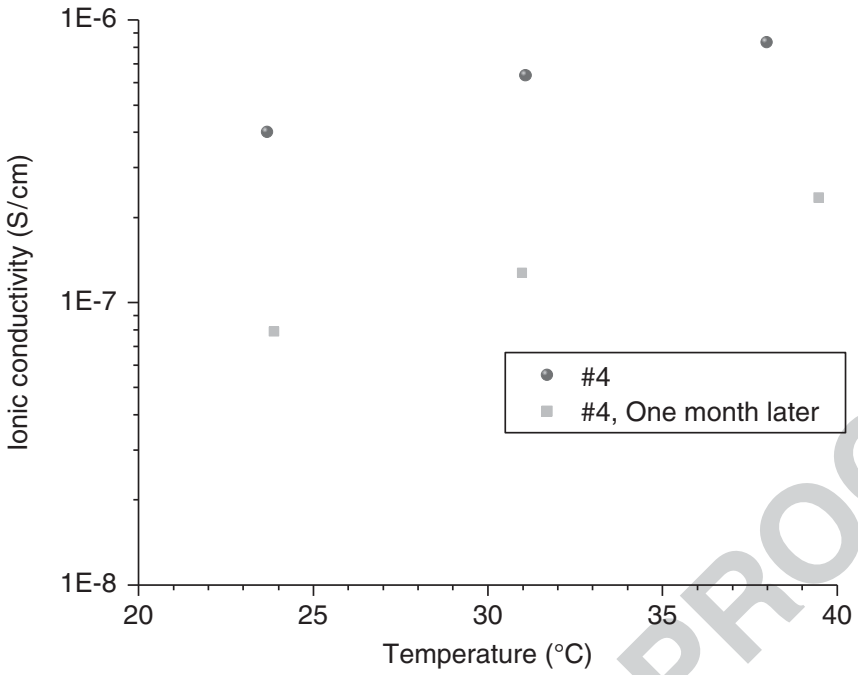

Fig. 20.32 Comparison of LIPON ionic conductivity 1 month later at air exposure

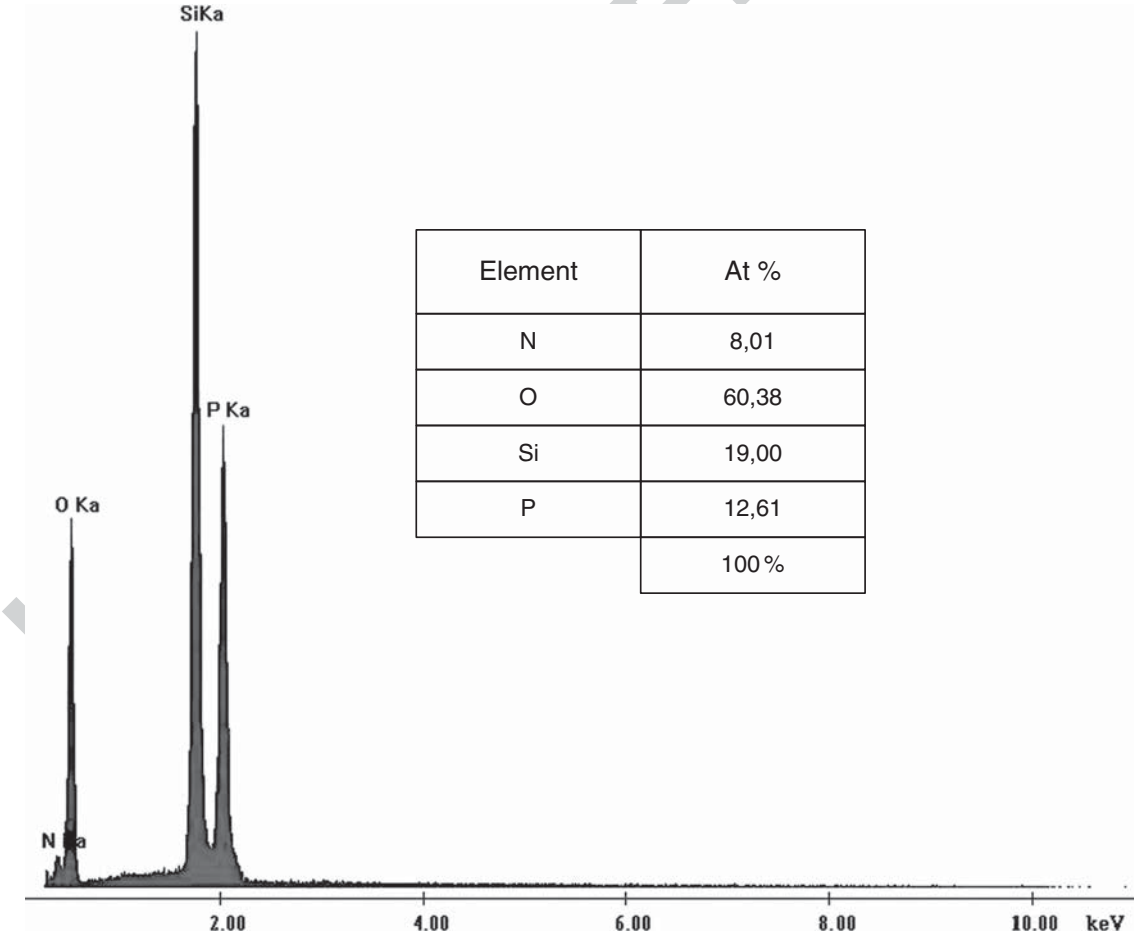

Element	At %
N	8,01
O	60,38
Si	19,00
P	12,61
	100 %

Fig. 20.33 EDX of LIPON film

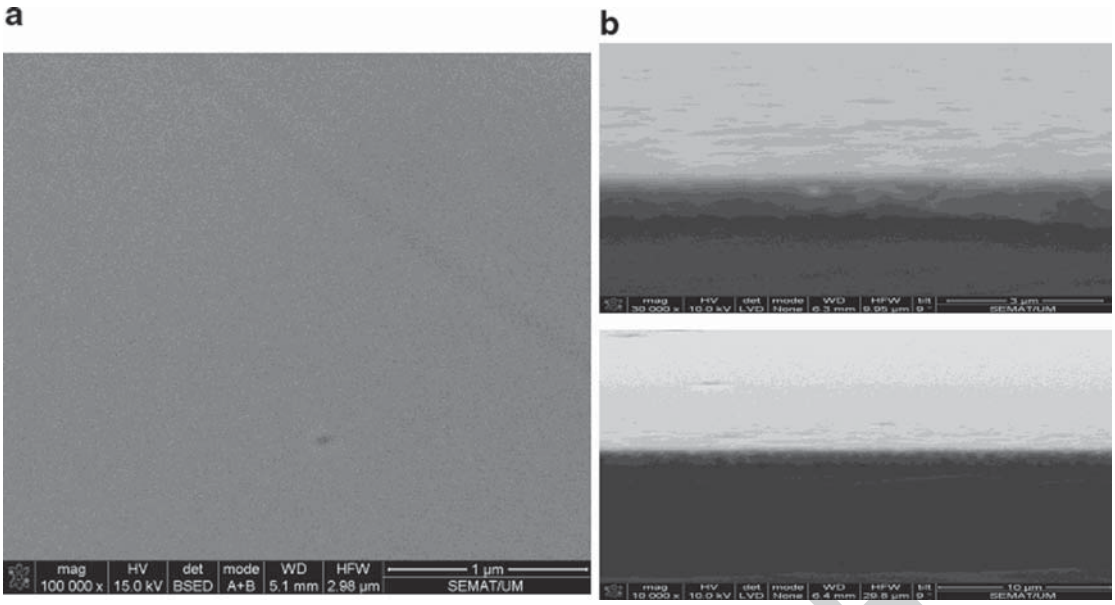

Fig. 20.34 LIPON SEM. (**a**) Surface picture, (**b**) cut images

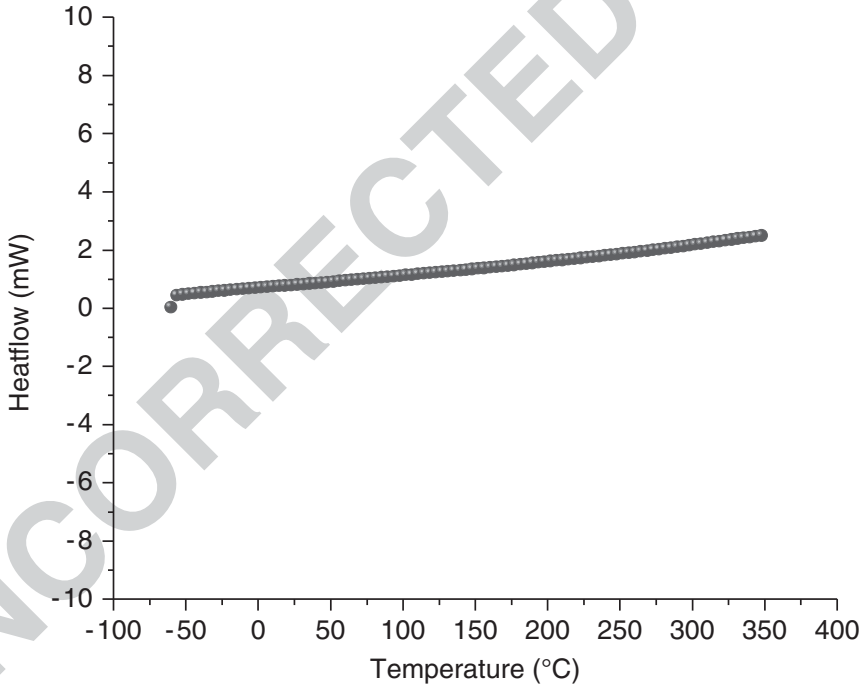

Fig. 20.35 Heat flow (mW) of LIPON film as a function of temperature during DSC analysis

increases with increasing temperature. The reduction of pressure and power source during the deposition increases the ionic conductivity. The graph of Fig. 20.31 shows the ionic conductivity of depositions "1," "3," and "4" as a function of pressure during deposition. 717 718 719 720

The ionic conductivity of sample "#4" was also measured after being exposed to the ambient atmosphere for a month (Fig. 20.32). It was concluded that the 721 722

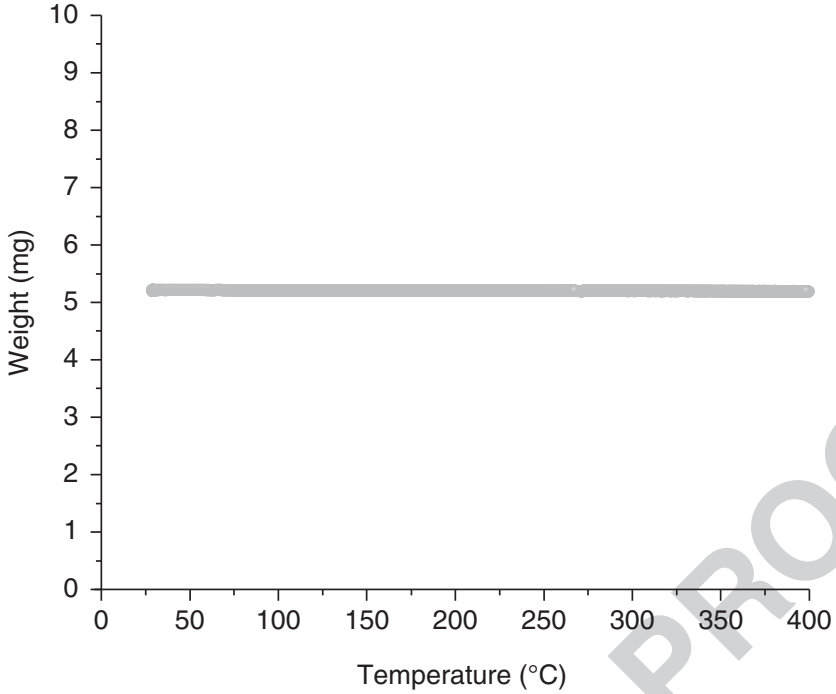

Fig. 20.36 Weight of LIPON film as a function of temperature during TGA analysis

behavior of the sample remained unchanged, but its ionic conductivity decreased considerably.

The chemical composition of LIPON film was also measured using EDX technique, where the oxygen has the largest share of atomic percentage (Fig. 20.33). Images of the surface and cut of LIPON samples were also generated by the SEM technique (Fig. 20.34). Note that the images do not show crystalline grains. The XRD analysis also confirmed the amorphous structure.

The thermal stability of LIPON films was also measured by Differential Scanning Calorimetry (DSC) and Themogravimetric analysis (TGA) techniques. Figure 20.35 shows the result obtained with DSC and Fig. 20.36 shows the result obtained from the TGA. It can be concluded from these graphs that the LIPON is stable when subjected to temperatures up to 400°C.

20.4.4 Anode

Initially, the lithium metal was the material chosen as the anode (negative electrode) of thin-film solid-state battery. This material was chosen due to the large amount of lithium ions that it can provide during battery discharge. Contacts were deposited on glass to measure resistance within the vacuum chamber and during deposition. Lithium was deposited by thermal evaporation and deposition parameters can be found in Table 20.12.

Table 20.12 Deposition parameters of anode

Thin-film	Deposition technique	Current source	Thickness (μm)	Resistance with 3 μm thickness (Ω)	t35.1
#01	Thermal		6.0	3.26	t35.2
#02	evaporation	150 A	5.3	3.04	t35.3
#03			3.3	3.50	t35.4

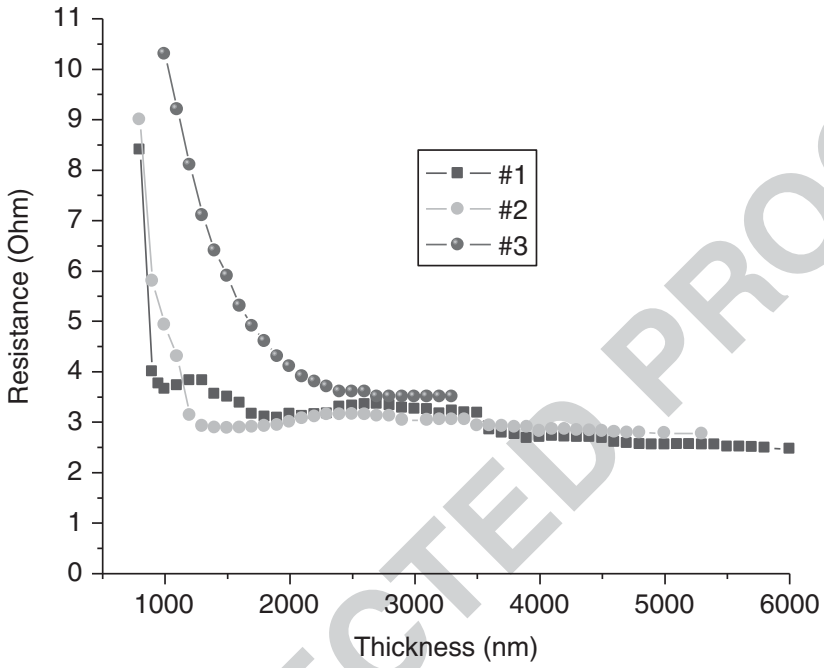

Fig. 20.37 Lithium resistance during deposition

The last column of Table 20.12 shows the resistance value measured when the lithium film reaches 3 μm thick. The graph of Fig. 20.37 shows resistance values measured during depositions. The resistance measurements were performed during the deposition with a four point setup.

After deposition, the resistance of lithium when it comes into contact with the atmosphere was investigated. The results in Fig. 20.38 show that lithium film oxidizes very quickly in contact with the ambient atmosphere and thus a protective film, deposited on top of lithium, is essential for battery functioning.

20.4.5 Battery Fabrication

The fabrication of solid-state lithium battery was projected using only shadow masks. The shadow masks are essential for fabrication of the battery to prevent short circuit between the battery electrodes owing to lack of lithography processes that can replace the shadow masks. The shadow mask to the battery current collectors

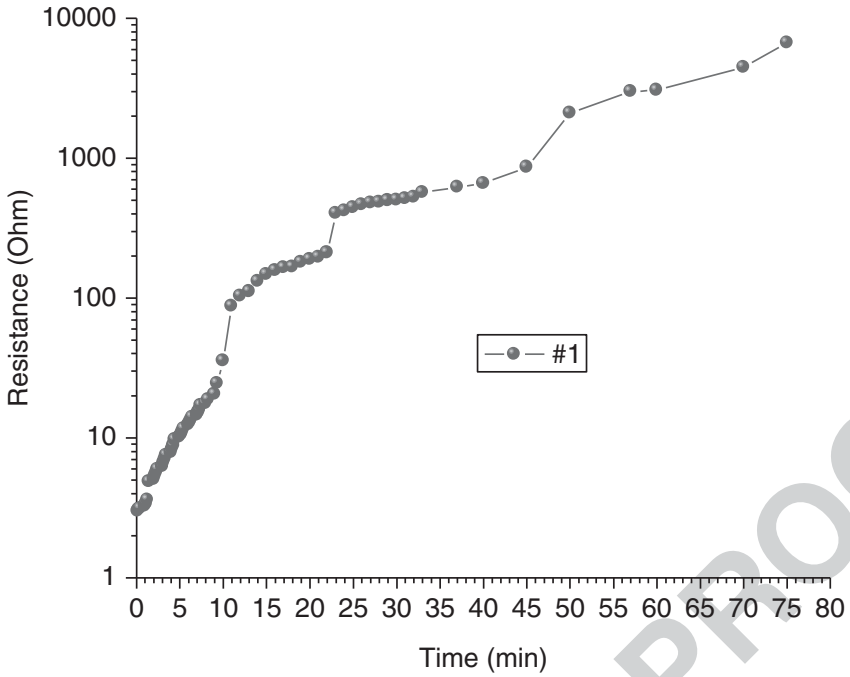

Fig. 20.38 Lithium resistance measured during ambient atmosphere exposure

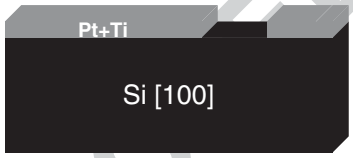

Fig. 20.39 Design of battery current collectors (thickness was exaggerated for better visualization)

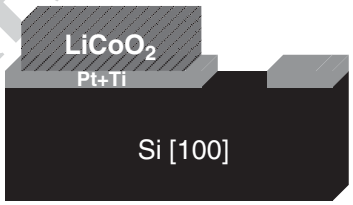

Fig. 20.40 Design of battery cathode (thickness was exaggerated for better visualization)

permits the contacts to have the format shown in Fig. 20.39. The cathode current collector is on the left side of the image and the anode current collector on the right side.

Then, the battery cathode is deposited as illustrated in Fig. 20.40, being connected only with the cathode current collector. This takes into account the area needed to connect an electric wire (left margin on the left).

After $LiCoO_2$ annealing, the electrolyte deposition is performed as shown in Fig. 20.41. The electrolyte fills the gap left by the previous mask to ensure isolation between the cathode and anode of the battery.

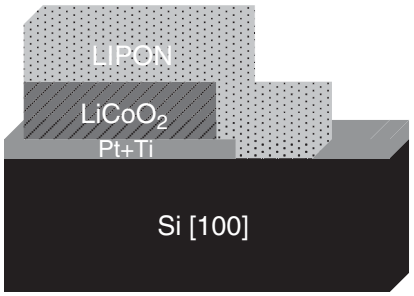

Fig. 20.41 Design of battery electrolyte (thickness was exaggerated for better visualization)

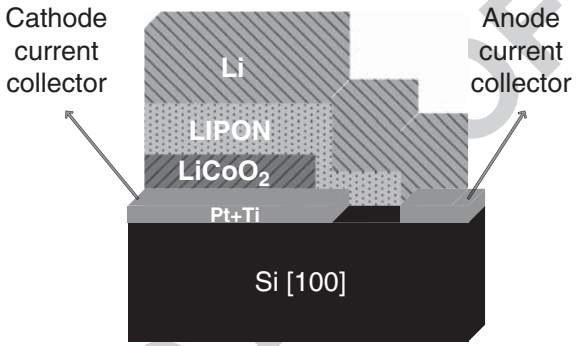

Fig. 20.42 Design of complete battery (thickness was exaggerated for better visualization)

The battery manufacture is completed with the deposition of the anode, as shown in Fig. 20.42. Figure 20.42 also indicates positive and negative battery contacts. Note that without a protective film deposited over the battery anode it cannot operate outside the vacuum chamber.

20.5 Conclusions

AQ2

The overall objective of this work was to select, fabricate, and characterize the materials to fabricate a lithium solid-state battery. A lithium battery is composed primarily of three materials, the cathode, electrolyte, and anode. The manufacturing process and design for the battery was projected. The results presented in this work fall within the above objectives, presenting the following solutions:

- Silicon substrate, to integrate the battery with microelectronics processes.
- Current collectors consisting of two thin films, 30 nm titanium and 70 nm platinum. With this solution the adhesion problem of platinum to silicon was eliminated. Unwanted reactions between the contacts and the electrodes are prevented by using platinum.
- Cathode (positive electrode) of lithium cobalt oxide ($LiCoO_2$) with a fully crystalline structure and high capacity for insertion/extraction of lithium ions.
- Electrolyte of lithium phosphorus oxynitride (LIPON) with high ionic conductivity and stable up to 400°C.
- Anode (negative electrode) of metallic lithium, which allows a high amount of lithium ions.

- Manufacturing process with different structures for each of the constituent materials of the battery, preventing contact between battery electrodes. Manufacture of films using shadow masks, due to lithography processes are not yet developed for the chosen materials.

20.5.1 $LiCoO_2$

$LiCoO_2$ is mostly used as cathode material in lithium batteries because of its excellent electrochemical stability, high capacity of lithium-ion diffusion, and capability to provide a high voltage to the battery. The fully crystalline structure facilitates the diffusivity of lithium ions and decreases the resistivity of the $LiCoO_2$. The $LiCoO_2$ film was deposited by RF sputtering and presented the best characteristics with a power source of 150 W, a pressure of 2×10^{-3} mbar, 40 sccm of argon, and an annealing at 650°C for 2 h in a vacuum. Electrical resistivity of 3.7 Ω-mm was achieved and chemical composition proven by EDX technique. A SEM image was also shown for the crystallization of $LiCoO_2$ film.

20.5.2 LIPON

LIPON is a glassy electrolyte with high ionic conductivity and high electrical resistivity. It has an electrical resistivity greater than $10^{14}\,\Omega$ and has an ionic conductivity of $6.3 \times 10^{-7}\,\mathrm{Sc\,m^{-1}}$ for a temperature of 26°C. The LIPON was deposited by RF sputtering with a power source of 150 W, pressure of 3×10^{-4} mbar and 20 sccm of nitrogen. The chemical composition and structure of the amorphous LIPON were proven using the EDX and SEM techniques. Thermal stability of LIPON up to 400°C was also proven using the DSC and TGA techniques.

20.5.3 Lithium

The lithium metal is the most common material used as battery anode due to the high amount of lithium ions that it can provide at battery discharge. This was deposited by thermal evaporation and its resistance measured during the deposition. The resistance of about 3.5 Ω was measured and the oxidation of the film in contact with the ambient atmosphere evaluated. The necessity of a protective film to prevent oxidation of lithium was proved.

20.6 Future Trends for Thin-Film Batteries

The fabrication and characterization of a battery using the process presented and optimized manufacturing revenues during this work will provide the desired goal in this area: a rechargeable solid-state battery, totally fabricated in thin-films. The battery characterization must take place within a vacuum chamber to prevent oxidation. Then, a material that protects the battery from the oxidation must be found and tested. The use of LIPON, silicon nitride, or Parylene as protection layer has been suggested. The substitution of metallic lithium as the anode of the battery by a material having a higher melting point will allow the welding processes on the battery. On the other hand, the use of nano-structured materials at the anode and cathode opens horizons for the development of batteries with times of charge/discharge of tens of seconds. The integration of the battery in microelectronics manufacturing processes would be the next step, aiming at their integration in integrated circuits.

References

1. T. Minami et al., *Solid State Ionics for Batteries* (Springer, New York, 2005)
2. N. Ariel, Integrated thin film batteries on silicon, Ph.D. thesis, Massachusetts Institute of Technology, Cambridge, 2005
3. K. Xu, Nonaqueous liquid electrolytes for lithium-based rechargeable batteries, Chem. Rev. **104**, 4303–4417 (2004)
4. F.S. Spear, The quantitative relationships among P, T, chemical potential, phase composition and reaction progress in igneous and metamorphic systems, Mineral. Petrol. **99**, 249–256 (1988)
5. A. Volta, On the electricity excited by the mere contact of conducting substances of different species, Philos. Trans. R. Soc. **90**, 289 (1800)
6. I. Buchmann, *Batteries in a Portable World* (Cadex Electronics Inc., Nuremberg, 1997)
7. P. Gallone, Galvani's frog: Harbinger of a new era, Electrochim. Acta **31**, 1485–1490 (1986)
8. M. Piccolino, The bicentennial of the voltaic battery (1800–2000): the artificial electric organ, Perspectives **23**, 147–151 (2000)
9. http://www.mpoweruk.com/history.htm Consulted on 23 May 2012
10. http://www.energizer.eu. Consulted on 23 May 2012
11. R. Moshtev, B. Johnson, State of the art of commercial Li ion batteries, J. Power Sources **91**, 86–91 (2000)
12. Y. Nishi, Lithium ion secondary batteries; past 10 years and the future, J. Power Sources **100**, 101–106 (2001)
13. K. Murata et al., An overview of the research and development of solid polymer electrolyte batteries, Electrochim. Acta **45**, 1501–1508 (2000)
14. http://www.cymbet.com/products/index.php. Consulted on 23 May 2012
15. M. Armand, J. Tarascon, Building better batteries, Nature **451**, 652–657 (2008)
16. A.S. Aricò et al., Nanostructured materials for advanced energy conversion and storage devices, Nat. Mater. **4**, 366–377 (2005)
17. L.F. Nazar et al., Nanostructured materials for energy storage, Int. J. Inorg. Mater. **3**, 191–200 (2001)

18. P.G. Bruce et al., Nanomaterials for rechargeable lithium batteries, Angew. Chem. Int. Ed. **47**, 2930–2946 (2008)
19. W.-Y. Li et al., Co_3O_4 nanomaterials in lithium-ion batteries and gas sensors, Adv. Funct. Mater. **15**, 851–857 (2005)
20. H. Chen et al., From biomass to a renewable $Li_XC_6O_6$ organic electrode for sustainable Li-ion batteries, ChemSusChem **1**, 348–355 (2008)
21. A. Patil et al., Issue and challenges facing rechargeable thin film lithium batteries, Mater. Res. Bull. **43**, 1913–1942 (2008)
22. K. Kanehori et al., Thin film solid electrolyte and its application to secondary lithium cell, Solid State Ionics **9–10**, 1445–1448 (1983)
23. I.E. Kelly et al., Poly(ethylene oxide) electrolytes for operation at near room temperature, J. Power Sources **14**, 13–21 (1985)
24. H. Ohtsuka and J. Yamaki, Preparation and electrical conductivity of $Li_2O - V_2O_5 - SiO_2$ thin films, J. Appl. Phys. **28**, 2264–2267 (1989)
25. H. Ohtsuka et al., Solid state battery with $Li_2O - V_2O_5 - SiO_2$ solid electrolyte thin film, Solid State Ionics **40–41**, 964–966 (1990)
26. M.M. Mojarradi et al., Power management and distribution for system on a chip for space applications, Jet Propulsion Laboratory, California Institute of technology, n.° 284
27. X. Yu et al., A stable thin-film lithium electrolyte: lithium phosphorus oxynitride, J. Electrochem. Soc. **144**, 524–532 (1997)
28. B. Wang et al., Characterization of thin-film rechargeable lithium batteries with lithium cobalt oxide cathodes, J. Electrochem. Soc. **143**, 3203–3213 (1996)
29. B.J. Neudecker et al., "Lithium-free" thin-film battery with in situ plated Li anode, J. Electrochem. Soc. **147**, 517–523 (2000)
30. Y.S. Park et al., All-solid-state lithium thin-film rechargeable battery with lithium manganese oxide, Electrochem. Solid-State Lett. **2**, 58–59 (1999)
31. M. Baba et al., Fabrication and electrochemical characteristics of all-solid-state lithium-ion batteries using V_2O_2 thin films for both electrodes, Electrochem. Solid-State Lett. **2**, 320–322 (1999)
32. M. Baba et al., Fabrication and electrochemical characteristics of all-solid-state lithium-ion rechargeable batteries composed of $LiMn_2O_4$ positive and V_2O_5 negative electrodes, J. Power Sources **97–98**, 798–800 (2001)
33. M. Baba et al., Multi-layered Li-ion rechargeable batteries for a high-voltage and high-current solid-state power source, J. Power Sources **119–121**, 914–917 (2003)
34. G. Meunier et al., New positive-electrode materials for lithium thin film secondary batteries, Mater. Sci. Eng. B **3**, 19–23 (1989)
35. S.S. Zhang, The effect of the charging protocol on the cycle life of a Li-ion battery, J. Power Sources **161**, 1385–1391 (2006)
36. N.J. Dudney et al., Nanocrystalline $Li_XMn_2 - YO_4$ cathodes for solid-state thin-film rechargeable lithium batteries, J. Electrochem. Soc. **146**, 2455–2464 (1999)
37. J.B. Bates et al., 5 volt plateau in $LiMn_2O_4$ thin films, J. Electrochem. Soc. **142**, L149–L151 (1995)
38. J.B. Bates et al., Thin-film rechargeable lithium batteries, J. Power Sources **54**, 58–62 (1995)
39. B.J. Neudecker et al., Lithium silicon tin oxynitride (Li_YSiTON): high-performance anode in thin-film lithium-ion batteries for microelectronics, J. Power Sources **81–82**, 27–32 (1999)
40. S.D. Jones, J.R. Akridge, A thin film solid state microbattery, Solid State Ionics **53–56**, 628–634 (1992)
41. http://www.infinitepowersolutions.com/. Consulted on 23 May 2012
42. J.O. Besenhard, *Handbook of Battery Materials* (Wiley, Weinheim, 1999)
43. F.M. Gray, *Solid Polymer Electrolytes: Fundamentals and Technological Applications* (VCH Publishers, New York, 1991)
44. M. Armand et al., *Extended Abstracts Second International Conference on Solid Electrolytes*, St Andrews, Scotland, 1978

45. J.-M. Tarascon, M. Armand, Issues and challenges facing rechargeable lithium batteries Nature **414**, 359 (2001)
46. F.M. Gray, *Polymer Electrolytes*, RSC Materials Monographs (Royal Society of Chemistry, London, 1997)
47. D.E. Fenton et al., Complexes of alkali metal ions with poly (ethylene oxide), Polymer **14**, 589 (1973)
48. P.G. Bruce (ed.), *Solid-State Electrochemistry* (Cambridge University Press, Cambridge, 1995)
49. P.M. Blonsky et al., Polyphosphazene solid electrolytes, J. Am. Chem. Soc. **106**, 6854–6855 (1984)
50. J.R. MacCallum, C.A. Vincent (ed.), *Polymer Electrolytes Reviews* (Elsevier Applied Science, London, 1987), pp. 1–22
51. R. Frech, S. Chintapalli, Effect of propylene carbonate as a plasticizer in high molecular weight PEO – $LiCF_3SO_3$ electrolytes, Solid State Ionics 61–85 (1996)
52. M.M. Silva et al., Study of novel lithium salt-based, plasticized polymer electrolytes, J. Power Sources **111**, 52–57 (2002)
53. M.M. Silva et al., Characterization of a novel polymer electrolyte based on a plasticizing lithium salt, in *Advanced Batteriesand Super Capacitors*, ed. by G. Nazri, R. Koetz, B. Scrosati, P.A. Moro, E.S. Takeuchi (The Electrochemical Society Proceedings Series PV2001-21, 2003), p. 476
54. CW Walker, M. Salomon, Improvement of ionic conductivity in plasticized PEO-based solid polymer electrolytes, J. Electrochem. Soc. **140**, 3409 (1993)
55. F. Alloin et al., Conductivity measurements of LiTFSI triblock copolymers with a central POE sequence, Electrochim. Acta **37**, 1729 (1992)
56. A.L. Pont et al., Pyrrolidinium-based polymeric ionic liquids as mechanically and electrochemically stable polymer electrolytes, J. Power Sources **188**, 558–563 (2009)
57. M. Armand et al., in *Second International Symposium on Polymer Electrolytes*, ed. by B. Scrosati (Elsevier Applied Science, New York, 1990), p. 91
58. W. Gorecki et al., Physical properties of solid polymer electrolyte PEO(LiTFSI) complexes, Phys. Condens. Matter **7**, 6823 (1995)
59. A. Vallée et al., Comparative study of poly(ethylene oxide) electrolytes made with $LiN(CF_3SO_2)_2$, $LiCF_3SO_3$ and $LiClO_4$: thermal properties and conductivity behaviour, J. Electrochim. Acta **37**, 1623 (1992)
60. M. Hernandez et al., Spectroscopic characterization of metal chloride/polyamide complexes, Ionics **1**, 454 (1995)
61. S. Lascaud et al., Phase diagrams and conductivity behavior of poly (ethylene oxide)-molten salt rubbery electrolytes, Macromolecules **27**, 7469 (1994)
62. F. Gray, *Polymer Electrolytes*, RSC Materials Monographs (The Royal Society of Chemistry, London, 1997)
63. S.S. Zhang et al., Understanding formation of solid electrolyte interface film on $LiMn_2O_4$ electrode, J. Electrochem. Soc. **149**, A586 (2002)
64. S.S. Zhang et al., A new approach toward improved low temperature performance of Li-ion battery, Electrochem. Commun. **4**, 928 (2002)
65. S.S. Zhang et al., Low-temperature performance of Li-ion cells with a $LiBF_4$-based electrolyte, J. Solid State Electrochem. **7**, 147 (2003)
66. P.C. Barbosa et al., Phase relationships and conductivity of the polymer electrolytes poly(ethylene oxide)/lithium tetrafluoroborate and poly(ethylene oxide)/lithium trifluoromethanesulfonate, J. Mater. Chem. **20**, 723 (2010)
67. S.M. Zahurak, M.L. Kaplan, E.A. Rietman, D.W. Murphy, R.J. Cava, Phase relationships and conductivity of the polymer electrolytes poly(ethylene oxide)/lithium tetrafluoroborate and poly(ethylene oxide)/lithium trifluoromethanesulfonate, Macromolecules **21**, 654 (1988)
68. M.M. Silva et al., Characterization of solid polymer electrolytes based on poly-(trimethylenecarbonate) and lithium tetrafluoroborate, Electrochim. Acta **49**, 1887 (2004)

69. G. Chiodelli et al., Ionic conduction and thermal properties of PEO-lithium tetrafluoro borate films, Solid State Ionics **28–30**, 1009 (1988)
70. M.B. Armand et al., *Fast Ion Transport in Solids* (Elsevier, Amsterdam, 1979), pp. 131–136
71. J.H. Correia, J.P. Carmo, Introdução às microtecnologias no silício, LIDEL, 2010, ISBN: 978-972-757-716-3
72. A.A.R. Elshabini-Riad, F.D. Barlow III, *Thin Film Technology Handbook* (McGraw-Hill Companies, New York, 1998)
73. N. Maluf, *An Introduction to Microelectromechanical Systems Engineering* (Artech House, London, 2000)
74. S.A. Campbell, *The Science and Engineering of Microelectronic Fabrication* (Oxford University Press, Oxford, 2001)
75. L. Gonçalves, Microssistema termoeléctrico baseado em teluretos de bismuto e antimónio, Ph.D. thesis, University of Minho, 2008
76. B.D. Cullity, S.R. Stock, *Elements of X-Ray Diffraction* (Addison-Wesley, New York, 1978)
77. http://www.purdue.edu/rem/rs/sem.htm Consulted on 23 May 2012
78. L.J. van der Pauw, A method of measuring the resistivity and Hall coefficient on lamellae of arbitrary shape, Philips Tech. Rev. **20**, 220–224 (1958)
79. Carlos Silva, Preparação e caracterização de electrólitos poliméricos, Ph.D. thesis, University of Minho, 1996
80. C.R.A. Catlow et al., An EXAFS study of the structure of rubidium polyethyleneoxide salt complexes, Solid State Ionics **9–10**, 1107–1113 (1983)
81. P.G. Bruce et al., Preliminary results on a new polymer electrolyte PEO − $Hg(ClO_4)_2$, Br. Polym. J. **20**, 193–194 (1988)
82. R.D. Armstrong, M.D. Clarke, Lithium ion conducting polymeric electrolytes based on poly(ethylene) adipate, Electrochim. Acta **29**, 1443–1446 (1984)
83. C.A. Vincent, Polymer electrolytes, Prog. Solid State Chem, **17**, 145–261 (1987)
84. M. Watanabe et al., Effects of polymer structure and incorporated salt species on ionic conductivity of polymer complexes formed by aliphatic polyester and alkali metal thiocyanate, Macromolecules **19**, 188–192 (1986)
85. F.M. Gray, *Polymer Electrolytes*, RSC Materials Monographs (The Royal Society of Chemistry, London, 1997)
86. M.E. Orazem, B. Tribollet, *Electrochemical Impedance Spectroscopy* (John Wiley & Sons, New York, 2008)
87. M. Plancha, Electrólitos poliméricos para sistemas electroquímicos de energia, Ph.D. thesis, Technical University of Lisbon, 2008
88. M.E. Brown, *Introduction to Thermal Analysis: Techniques and Applications* (Kluwer Academic, Dordrecht, 2001)
89. K. Sreenivas et al., Investigation of Pt/Ti bilayer metallization on silicon for ferroelectric thin film integration, J. Appl. Phys. **75**, 232–239 (1994)
90. C.Y. Ting, M. Wittmer, The use of titanium-based contact barrier layers in silicon technology, Thin Solid Films **96**, 327–345 (1982)
91. S.L. Firebaugh et al., Investigation of high-temperature degradation of platinum thin films with an in situ resistance measurement apparatus, J. Microelectromech. Syst. **7**(1), 128–135 (1998)
92. M.-S. Park, Performance evaluation of printed $LiCoO_2$ cathodes with PVDF-HFP gel electrolyte for lithium ion microbatteries, Electrochim. Acta **53**, 5523–5527 (2008)
93. L. Predoana, Electrochemical properties of the $LiCoO_2$ powder obtained by sol-gel method, J. Eur. Ceram. Soc. **27**, 1137–1142 (2007)
94. L. Predoana et al., Advanced techniques for $LiCoO_2$ preparation and testing, in *Proceedings of the International Workshop*, Sofia, Bulgaria, 4–9 September de 2004
95. H.Y. Park et al., Bias sputtering and characterization of $LiCoO_2$ thin film cathodes for thin film microbattery, Mater. Chem. Phys. **93**, 70–78 (2005)
96. Powder Diffraction File, Joint Committee on Powder Diffraction Standards, ASTM, Philadelphia, 1967

97. J.B. Bates et al., Thin-film lithium and lithium-ion batteries, Solid State Ionics **135**, 33–45 (2000)
98. Y. Hamon et al., Influence of sputtering conditions on ionic conductivity of LIPON thin films, Solid State Ionics **177**, 257–261 (2006)
99. N.J. Dudney, B.J. Neudecker, Solid state thin-film lithium battery systems, Solid State Mater. Sci. **5**, 479–482 (1999)
100. N.J. Dudney, Solid-state thin-film rechargeable batteries, Mater. Sci. Eng. B **116**, 245–249 (2005)
101. H.Y. Park et al., Effects of sputtering pressure on the characteristics of lithium ion conductive lithium phosphorous oxynitride thin film, J. Electroceram **17**, 1023–1030 (2006)

Acknowledgements

This work was financial supported by FEDER/COMPETE and FCT funds with the project PTDC/EEAELC/114713/2009 and with first author scholarship SFRH/BD/78217/2011.

AUTHOR QUERIES

AQ1. The sentence beginning “It was also proven ...” has been modified to begin as “The thermal stability ...”. Please confirm the edits are ok.
AQ2. Please check the identified heading levels for correctness.